Identifying Disease Foci from Static and Dynamic Effective Connectivity Networks: Illustration in Soldiers with Trauma

D. Rangaprakash [1,2] Michael N. Dretsch,[3,4] Archana Venkataraman,[5] Jeffrey S. Katz,[2,6,7] Thomas S. Denney, Jr,[2,6,7] and Gopikrishna Deshpande [2,6,7]*

[1]*AU MRI Research Center, Department of Electrical and Computer Engineering, Auburn University, Auburn, AL, USA*
[2]*Department of Psychiatry and Biobehavioral Sciences, University of California Los Angeles, Los Angeles, CA, USA*
[3]*U.S. Army Aeromedical Research Laboratory, Fort Rucker, Alabama*
[4]*Human Dimension Division, HQ TRADOC, Fort Eustis, Virgina*
[5]*Department of Electrical and Computer Engineering, Johns Hopkins University, Baltimore, Maryland*
[6]*Department of Psychology, Auburn University, Auburn, Alabama*
[7]*Alabama Advanced Imaging Consortium, USA*

Abstract: Brain connectivity studies report group differences in pairwise connection strengths. While informative, such results are difficult to interpret since our understanding of the brain relies on region-based properties, rather than on connection information. Given that large disruptions in the brain are often caused by a few pivotal sources, we propose a novel framework to identify the sources of functional disruption from effective connectivity networks. Our approach integrates static and time-varying effective connectivity modeling in a probabilistic framework, to identify aberrant foci and the corresponding aberrant connectomics network. Using resting-state fMRI, we illustrate the utility of this novel approach in U.S. Army soldiers ($N = 87$) with posttraumatic stress disorder (PTSD), mild traumatic brain injury (mTBI) and combat controls. Additionally, we employed machine-learning classification to identify those significant connectivity features that possessed high predictive ability. We identified three disrupted foci (middle frontal gyrus [MFG], insula, hippocampus), and an aberrant prefrontal-subcortical-parietal network of information flow. We found the MFG to be the pivotal focus of network disruption, with aberrant strength and temporal-variability of effective connectivity to the insula, amygdala and hippocampus. These connectivities also possessed high predictive ability (giving a classification accuracy of 81%); and they exhibited significant associations with symptom severity and neurocognitive functioning. In summary, dysregulation originating in the MFG caused elevated and temporally less-variable connectivity in subcortical regions, followed by a similar effect on parietal memory-related regions. This mechanism likely contributes to the reduced control over traumatic

Additional Supporting Information may be found in the online version of this article.

*Correspondence to: Gopikrishna Deshpande, AU MRI Research Center, Department of Electrical and Computer Engineering, Auburn University, 560 Devall Dr, Suite 266D, Auburn, AL 36849, USA. E-mail: gopi@auburn.edu

Disclosures: The authors report no competing interests.

Received for publication 14 February 2017; Revised 29 August 2017; Accepted 1 October 2017.

DOI: 10.1002/hbm.23841

Published online 00 Month 2017 in Wiley Online Library (wileyonlinelibrary.com).

memories leading to re-experiencing, hyperarousal and flashbacks observed in soldiers with PTSD and mTBI. *Hum Brain Mapp 00:000–000, 2017.*

Key words: Functional MRI; effective connectivity; dynamic connectivity; disease foci; posttraumatic stress disorder; mild traumatic brain injury; machine learning

INTRODUCTION

Brain imaging provides insight into the functional neuroarchitecture associated with psychiatric conditions such as mild traumatic brain injury (mTBI) and posttraumatic stress disorder (PTSD) [Costanzo et al., 2014], both prevalent in military service members. However, much of our understanding of the brain is organized around properties of neural regions, whereas our knowledge of the complex connections between the various regions is not as mature. Given that connectivity contains mechanistically pertinent information, which is different from what is available through functional magnetic resonance imaging (fMRI) activation studies, attaining region-specific information from connectivity data could advance our understanding of the neural circuitry and associated brain processes. Hence, we developed a novel framework to identify compromised pathological foci from directional brain networks, which likely represent the source(s) of network disruption in a given disorder. We illustrate the approach with fMRI data obtained from soldiers with PTSD and postconcussion syndrome (PCS, a chronic outcome of mTBI).

Exposure to blasts and subsequent head injuries result in mTBI, which has a high comorbidity with PTSD [Hoge et al., 2008, 2009]. As of September 2014, over 2.7 million Americans have served in Iraq and Afghanistan, of whom about 20% developed PTSD, 19% acquired TBI, and 7% acquired both [Veterans statistics: PTSD, Depression, TBI, Suicide, n.d.]. With current diagnostic procedures and treatments centering on subjective assessments, a thorough understanding of the mechanistic basis for both PTSD and PCS symptom presentation is essential for accurate diagnosis, targeted treatments, and return-to-duty decision making. Due to the largely overlapping symptomatology between PCS and PTSD [Eierud et al., 2014], it is imperative that objective connectivity markers of the respective neuropsychiatric and neurologic conditions are identified and validated to improve clinical evaluation and treatment outcomes. Prior fMRI works on comorbid PTSD and mTBI are limited [Spielberg et al., 2015], although its prevalence is considerably high in general society as well as military populations [Veterans statistics: PTSD, Depression, TBI, Suicide, n.d.]. In this work, we study group-level differences in brain networks between participants diagnosed with PTSD, PCS + PTSD (comorbid group diagnosed with both PCS and PTSD) and matched healthy combat controls.

Several studies have identified [Simmons and Matthews, 2012] certain key frontal and subcortical areas, among others, and associated connections which are impaired in both PTSD and PCS. However, a mechanistic explanation of the affected network architecture in PTSD with and without PCS is still under development. Specifically, given that network disruption often arises from aberrations in a few focal areas, segregation of such sources of network disruption from the connectivity changes that happen as a consequence of them, has been elusive. Since such foci are part of the affected network, the disruption is propagated to other regions connected with the foci. Therefore, we investigate the foci of network disruption, in addition to characterizing connectivity aberrations associated with them.

While functional connectivity (FC) is popularly used to study brain networks, there is a need to identify networks with causal relationships. Underlying network interactions could be causal in nature in addition to (or rather than) being synchronous, which are shown to exist even in fMRI timescales [Deshpande and Hu, 2012]. As such, it is important to discover causal networks in addition to coactivation networks for a more complete characterization. PTSD and PCS are generally seen as frontal dysregulation disorders [Simmons and Matthews, 2012], in which directional (or causal) influences originating from frontal areas are impaired. This further motivated us to employ directional causal connectivity or effective connectivity (EC). Surprisingly, there have been no fMRI studies that have investigated effective connectivity in either PTSD or mTBI or the comorbid condition.

EC refers to directional relationships among brain regions [Deshpande and Hu, 2012]. Granger causality (GC) is an exploratory technique used to quantify EC between brain regions [Deshpande et al., 2010a,b]. It is the most widely used approach to quantify causal influences in natural systems [Kirchgässner et al., 2012] including, but not limited to, epidemiology, molecular biology, econometrics, evolutionary biology, climate science, computer networks, linguistics, and brain science [Illari et al., 2011]. While GC involves assumptions and parameter choices, it has the advantage that it is a data driven approach and there are no requirements for specifying connectivity priors like in dynamic causal modeling (DCM) [Deshpande and Hu, 2012; Deshpande et al., 2012; Friston et al., 2013; Roebroeck et al., 2005]. While a wide range of applications take advantage of DCM, it would be practically impossible to build a DCM model with priors for whole-brain connectivity, as it would be computationally not feasible [Lohmann et al., 2012]. Both recent simulations [Ryali et al., 2011;

Wen et al., 2013] and experimental results [David et al., 2008; Katwal et al., 2013; Ryali et al., 2016] indicate that GC applied after deconvolving the HRF from fMRI data (as we have done), is reliable for making inferences about directional influences between brain regions. This method has also been employed in several recent fMRI studies [Bellucci et al., 2017; Deshpande et al., 2013; Feng et al., 2015; Grant et al., 2014, 2015; Hutcheson et al., 2015; Lacey et al., 2014; Sathian et al., 2013; Wheelock et al., 2014].

Most studies investigate EC or directional brain connectivity by assuming connectivity to be temporally stationary. Dynamic fluctuations of connectivity are not captured when using static connectivity. Given that mental processes happen within a few milliseconds to seconds' time, while an entire fMRI scan lasts for several minutes, it is natural that connectivity fluctuates over time, reflecting changing mental states, and that such variations carry biologically relevant information [Hutchison et al., 2013], which is distinct from that represented by static connectivity [Jia et al., 2014]. Some studies have even reported that connectivity dynamics are a better predictor of disease states than static connectivity [Jin et al., 2017]. Connectivity dynamics has been found to be a unique and important marker of brain functioning [Hansen et al., 2015]. Previous studies in PTSD and PCS have not utilized dynamic connectivity information in a manner that extends our understanding based on the information obtained from conventional static connectivity. In this study, we used static EC (SEC) as well as dynamic EC (DEC) measures [Wheelock et al., 2014].

Upon obtaining these whole-brain connectivities, we employed a probabilistic framework to identify affected foci, i.e., regions that are the likely primary sources of network disruption. This technique would also inform us on the underlying disrupted directional network associated with the disrupted foci. We adopted the technique developed recently for FC data [Venkataraman et al., 2013], and made specific modifications to the model formulation to make it suitable for both EC and dynamic connectivity data. The modifications were necessary because the probability distributions of EC and FC metrics are different (EC distribution is narrower), in addition to the fact that, unlike FC, EC is directional in nature. The technique is based on the concept that affected foci are associated with a large number of affected connections. It identifies compromised foci and also provides associated compromised connections.

We constructed separate brain networks using strength (SEC) and temporal variability (variance of DEC [vDEC]) of directional connectivity, and then used them to identify diseased foci separately. The obtained foci for SEC and vDEC were then overlapped (intersection) to obtain final foci which had both aberrant SEC and vDEC in the clinical groups. Here onward, we would use the term "clinical groups" instead of referring every time as "in PTSD and PCS + PTSD." The compromised connections associated with the foci were obtained and overlapped in a similar manner, but with certain restrictions as described next.

It has been shown that lower temporal variability of connectivity is associated with both neurologic and psychiatric conditions [Garrett et al., 2013; Jia et al., 2014; Miller et al., 2016; Rangaprakash et al., 2016, 2017a,b,c; Rashid et al., 2016], often presenting as a lack of cognitive flexibility. Reduced temporal variance in DFC is associated with psychiatric disorders as well as compromised behavioral performance in healthy individuals [Jia et al., 2014; Sakoğlu et al., 2010]. We suggest that this reduction is associated with compromised ability to dynamically adjust (e.g., behavior, thoughts, etc.) to changing conditions. Such a phenomenon is widely recognized in other biological systems, for example, reduction in heart rate variability is a marker of cardiovascular disease [Greiser et al., 2009]. Since environmental factors and bodily internal states are changing continuously, a healthy biological system adapts its activity in real-time to accommodate such changes. In these terms, a connectivity path less variable across time reflects compromised brain health. Such connectivity characterization has been employed in recent works, with higher connectomic flexibility being associated with favorable/better task performance in healthy adults [Jia et al., 2014] and psychiatric disorders [Rangaprakash et al., 2015, 2017a]. Higher variability of connectivity is also considered a marker of greater mental flexibility [Zhang et al., 2016]. In this work, we identified connections with altered SEC and lower vDEC in the clinical groups compared to controls.

Additionally, we presented in our earlier study that the PCS + PTSD group was found to be a more severe group compared to the PTSD group (in terms of symptom severity scores), owing to the added burden of mTBI [Rangaprakash et al., 2017a,b,c]. It is noteworthy that mTBI is a result of pressure waves arising from blasts and other non-blast events like vehicle accidents, while PCS is a behavioral syndrome, which is a consequence of the injury. Therefore, unlike TBI wherein the spatial location of injury can be different across subjects, the common behavioral manifestations among subjects with PTSD and mTBI suggests that it is likely to have common sources of neural network disruption in their brains. In addition, evidence shows that PCS increases the severity of PTSD [Vasterling et al., 2009]. Hence, we looked for connectivity paths associated with the affected foci, which had reducing vDEC and altered (either monotonically reducing or monotonically increasing) SEC as we moved from Control to PTSD to PCS + PTSD. We hypothesized that PTSD with and without PCS is characterized by certain affected regional foci, and those foci are associated with connections having altered strength (SEC) and lower variability (vDEC) of directional brain connectivity (see Fig. 1 for an illustration of our hypothesis). Additionally, we hypothesized that (secondary hypothesis) these connectivities are better predictors of the disorders than the available nonimaging

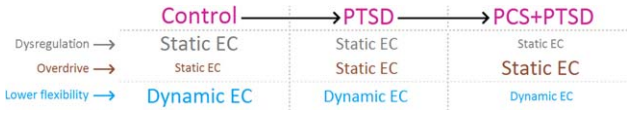

Figure 1.

Illustration of our hypothesis showing monotonically decreasing temporal variability of dynamic effective connectivity, and either increasing (overdrive) or decreasing (dysregulation) static effective connectivity as we move from Control to PTSD to PCS + PTSD. Font sizes are symbolic of the increasing/decreasing trend. [Color figure can be viewed at wileyonlinelibrary.com]

measures. We associated the connectivity paths exhibiting lower SEC with dysregulation, given that reduced engagement of certain prefrontal-cortical and prefrontal-subcortical connectivities is seen as a consequence of impaired regulation from prefrontal regions [Gross, 2014]. Similarly, we associated the connectivity paths exhibiting higher SEC with overdrive, or pathologically enhanced engagement, given that hyper-connectivity is considered as a response to neurological disruption [Hillary et al., 2015], and has been observed in individuals with PTSD [Cisler et al., 2014; Hayes et al., 2012; Simmons and Matthews, 2012]. The use of the word "overdrive" in such a context is not new, and has been prevalent in the literature [Modinos et al., 2017; Reiss et al., 2008]. The foci were identified using whole-brain connectivity data without imposing any priors, while the affected connectivity paths conforming to our hypothesis were restricted to those connections that were associated with the foci. Notably, we tested the hypothesis in a data-driven manner using resting-state fMRI, which is not task dependent.

For the connectivities that fit our hypothesis, we sought to assess their behavioral relevance; specifically, we tested the association of connectivity values with neurocognitive scores and symptom severity in PTSD and PCS.

Our hypothesis is based on an analysis framework, which relies on statistical separation between groups. However, statistical separation of between-group connectomics does not necessarily imply that they have predictive diagnostic ability [Deshpande et al., 2010a,b]; that is, they may not be able to predict group membership at an individual level with reasonable accuracy. Consequently, those connections that are both statistically significant and possess the discriminative power to classify subjects with high accuracy are more powerful. Several studies report successfully using machine learning classifiers on fMRI data for diagnostic prediction, including, but not limited to, major depressive disorder [Deshpande et al., 2009], Parkinson's disease [Marquand et al., 2013], PTSD [Liu et al., 2015], dementia [Chen et al., 2011], autism [Deshpande et al., 2013], ADHD [Deshpande et al., 2015] and prenatal cocaine exposure syndrome [Deshpande et al., 2010a,b]. However, to the best of our knowledge, there have been no studies that have used connectivity markers for the classification of both PTSD and PCS subjects. For psychiatric disorders like PTSD and PCS, classification using neuroimaging signatures could be employed to obtain more accurate diagnoses by assisting the clinician with additional information. Therefore, we employed a machine learning technique, which, in a data-driven fashion, recursively eliminates unimportant connectivity features from whole-brain connectivity data to identify those SEC and vDEC features that can predict the diagnostic membership of a novel subject with high accuracy. We specifically investigated whether there was an overlap between connectivities satisfying our primary hypothesis (Fig. 1) and those identified as having high predictive ability using machine learning. As stated earlier, we hypothesized that (secondary hypothesis) these connectivities will better predict the diagnostic membership of a novel subject than the available nonimaging measures (behavioral, neurocognitive and self-report measures), thus highlighting their relevance to the neuropathology of PTSD and PCS. We lay emphasis on the compromised foci and their associated connections that have high statistical separation as well as high predictive ability in addition to having behavioral relevance.

METHODS

A schematic of the entire processing pipeline is available at the end of the methods section (Fig. 5).

Participants

Active-duty U.S. Army soldiers (aged between 18 and 50 years) were recruited from Fort Rucker, AL, USA and Fort Benning, GA, USA to voluntarily participate in the study. The study was conducted in accordance with the Declaration of Helsinki. The procedures were approved by Auburn University's Institutional Review Board (IRB), and the Headquarters U.S. Army Medical Research and Materiel Command, IRB (HQ USAMRMC IRB).

Eighty-seven male, active-duty U.S. Army soldiers were enrolled in the study, which included 17 with PTSD, 42 with both PTSD and PCS (PCS + PTSD), and 28 combat controls (all groups matched in age, race and education), all having combat experience in Afghanistan (Operation Enduring Freedom, OEF) and/or Iraq (Operation Iraqi Freedom, OIF). Participants were grouped based on postconcussive symptoms using the Neurobehavioral Symptom Inventory (NSI) score, PTSD symptom severity using the PTSD Checklist-5 (PCL5) score, clinician referral and medical history. (i) Participants with no history of mTBI in the last five years, a total score ≥ 38 on the PCL5 and < 26 on the NSI were grouped as posttraumatic stress group (PTSD group). (ii) Participants with a history of medically documented mTBI, postconcussive symptoms, and scores ≥ 38 on the PCL5 and ≥ 26 on the NSI were grouped as the comorbid PCS + PTSD group. (iii) Participants with a score < 38 on the PCL5 and < 26 on the NSI, no DSM-IV-

TR or DSM-V diagnosis of a psychiatric disorder, no mTBI within the last 5 years, and no history of a moderate-to-severe TBI, were grouped as combat controls. None of the participants had a reported or documented diagnosis of substance dependency, mood and/or personality disorder. All participants reported being deployed to a combat environment. Time since the most recent mTBI was no earlier than three months and within the last five years for the PCS + PTSD group. PCL5 scores were significantly different between the control group and the PTSD and PCS + PTSD groups combined ($F(1, 172) = 20.6443$, $P = 3.64 \times 10^{-44}$). Such a comparison was done since PTSD is the common factor between PCS + PTSD and PTSD groups, and PCL5 score reflects only PTSD symptom severity. Similarly, NSI scores were significantly different between the PCS + PTSD group and the PTSD and control groups combined ($F(1, 172) = 32.6878$, $P = 1.32 \times 10^{-29}$).

Measures

Prior to their MRI scan, a battery of psychological health measures were administered to the participants, which consisted of the PTSD Checklist-5 (PCL-5; [Blevins et al., 2015]), Brief Traumatic Brain Injury Screen (BTBIS; [Schwab et al., 2007]), Neurobehavioral Symptom Inventory (NSI; [Cicerone and Kalmar, 1995]), Combat Exposure Scale (CES; [Guyker et al., 2013]), Life Events Checklist (LEC; [Gray et al., 2004]), Childhood Environment (CE;[King et al., 2003]), Zung Anxiety Scale (ZAS; [Zung, 1971]), Zung Depression Scale (ZDS; [Zung et al., 1965]), the Epworth Sleepiness Scale (ESS; [Johns, 1991]), and Alcohol Use Dependency Identification Test (AUDIT;[Saunders et al., 1993]). We next present, in further detail, those measures that were considered most relevant for the current study.

PTSD checklist-5 (PCL5, [Dickstein et al., 2014])

PCL5 is a 20-item self-report measure that assesses DSM-5 symptoms of PTSD. It has a variety of purposes like screening individuals for PTSD, making PTSD diagnoses and monitoring symptom change during and after treatment. Items are rated using a 5-point Likert scale; 1 = "Not at all" through 5 = "Extremely." A total symptom severity score (range: 20–100) is obtained by summing the scores for each of the 20 items, with a cut score of 38 for a precursory diagnosis of PTSD [Weathers et al., 2015]. PCL5 has been shown to be able to differentiate between soldiers with PTSD and healthy controls [Dretsch et al., 2016].

Neurobehavioral symptom inventory (NSI, [Cicerone and Kalmar, 1995])

This 22-item self-report questionnaire is designed to assess postconcussive symptoms in individuals who have sustained a TBI. Participants rate the severity of each symptom within the past month on a 5-point Likert scale, ranging from 0 (none) to 4 (very severe). The score (range: 0–88) is obtained by summing the individual scores of the 22 items.

CNS-Vital Signs® (CNS-VS, [Gualtieri and Johnson, 2006])

CNS-VS is a computerized neurocognitive assessment battery. In this work, we used five CNS-VS sub-tests (verbal memory, symbol digit coding, Stroop test, continuous performance test, and shifting attention test). The following CNS-VS domain scores were calculated: verbal memory (VM), complex attention (CA), reaction time (RT), processing speed (PS), cognitive flexibility (CF), and executive functioning (EF). Domain scores possess a mean of 100 and standard deviation of 15, which were averaged to form a single score or neurocognitive composite index (NCI) [Gualtieri and Johnson, 2006].

Procedures

Participants arriving at the research lab for their scheduled testing appointment were re-screened for eligibility, thoroughly screened for MRI contraindications and re-consented to ensure full comprehension of the study's procedures, benefits and their rights.*fMRI*: Participants were scanned in a 3T MAGNETOM Verio scanner (Siemens Healthcare, Erlangen, Germany) using T2* weighted multiband echo planar imaging (EPI) sequence in resting-state (the participants were required to keep their eyes open and not think of anything specific, and fixated on a white cross displayed in dark background on the screen using an Avotec projection system), with TR = 600 ms, TE = 30 ms, FA = 55°, slice gap = 1 mm, anterior to posterior phase encoding direction, voxel size= $3 \times 3 \times 4$ mm^3, multiband factor = 2 and 1,000 volumes. Brain coverage was limited to cerebral cortex, subcortical structures, midbrain and pons (with cerebellum being excluded). For each participant, two identical but separate scans were done and were processed independently, hence providing 174 sessions of resting-state data for the 87 participants. Mathematically this boosted the statistical power of our analysis beyond what would have been possible from single scans of 87 participants, since statistics were carried out with connectivity values which were double the number (per connectivity path) in comparison to the number of participants in each group.

Data Analysis

Nonimaging measures

Mean, median, range and standard deviation were calculated for self-report and neurocognitive measures. Ordinal data were analyzed using Kendall's Tau B (τb) test, and separate one-way analyses of variance (one-way ANOVA) with Dunnett's C correction for multiple comparisons were

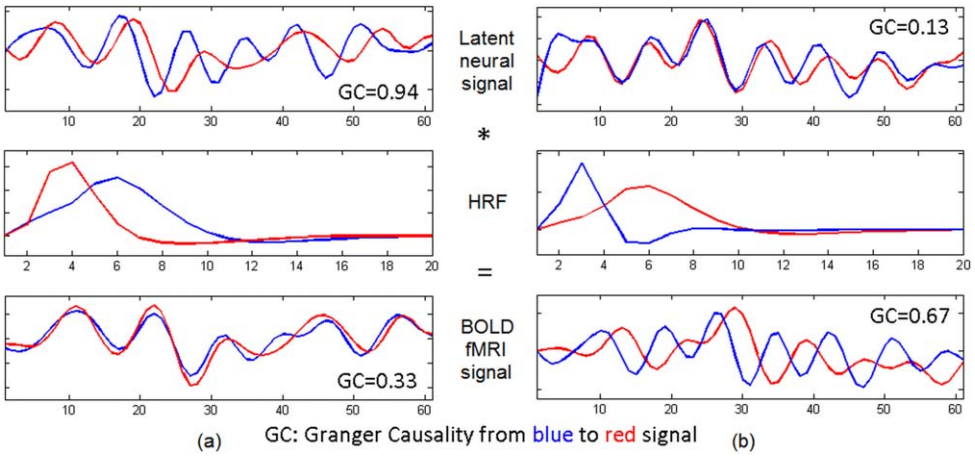

Figure 2.

Illustration of the importance of performing hemodynamic deconvolution, using two time series from our real fMRI data. The latent neural signals were convolved with the hemodynamic response function (HRF) to give the BOLD fMRI time series. Within-subject HRF variability across the brain could potentially give rise to a scenario wherein, **(a)** the underlying neural signals have true high directional connectivity (measured using Granger causality [GC] from blue to red signal, wherein it is evident that the red signal consistently follows after the blue signal) while the BOLD fMRI time series show low GC value, and **(b)** the latent neural signals have true low directional connectivity while the BOLD fMRI time series show high GC value. In the former case, the delay observable in the neural signals (red signal leads blue) is negated by the delay in the HRF (blue signal leads red) to give nearly overlapping BOLD time series. In the latter case, while the neural signals are nearly overlapping, the delay in the HRF results in an observable delay in the BOLD time series. [Color figure can be viewed at wileyonlinelibrary.com]

evaluated when comparing continuous variables between groups.

fMRI data preprocessing

Standard resting-state fMRI preprocessing steps were carried out, including realignment, normalization to MNI space, detrending and regressing out nuisance covariates such as six head-motion parameters, white matter signal and cerebrospinal fluid signal, and temporal band-pass filtering (0.01–0.1 Hz). The maximum allowed head-motion was half of the voxel size (1.5 mm), with no significant group differences in participant head motion ($P > 0.05$). Preprocessing was carried out using Data Processing Assistant for Resting-State fMRI (DPARSF, v1.7) [Chao-Gan and Yu-Feng, 2010], which is based on Statistical Parametric Mapping (SPM8) [Friston et al., 2007] and Resting-State fMRI Data Analysis Toolkit [Song et al., 2011].

The data were temporally normalized, rendering each timeseries with zero mean and unit variance. Deconvolution was then performed on voxel-wise data, since confounds emerging from inter-subject and spatial variability of the hemodynamic response function (HRF) [Handwerker et al., 2004] could give rise to a scenario wherein two fMRI timeseries have high directional connectivity while the underlying neural variables do not and vice versa (please refer to Fig. 2 for an illustration). Differences in HRF have been specifically reported in the case of PTSD and PCS, and such differences have been shown to impact connectivity findings [Rangaprakash et al., 2017a,b,c]. Further, causal connections could readily switch directions if the underlying HRFs have different time-to-peak. To this effect, it has been shown that deconvolution produces improved estimation of effective connectivity [David et al., 2008; Ryali et al., 2012]. In fact, a recent paper presenting the viewpoint of cellular neuroscience on BOLD fMRI [Hall et al., 2016] discussed about several caveats in interpreting fMRI findings that deserve careful consideration based on the underlying cellular mechanisms. One such chief issue pertains to neurovascular dynamics or HRF variability, about which they say as follows: "advances in cellular neuroscience demonstrating differences in this neurovascular relationship in different brain regions, conditions or pathologies are often not accounted for when interpreting BOLD." They suggest the use of computational modeling (e.g., deconvolution) to mitigate the issue.

We employed a popular blind deconvolution algorithm [Wu et al., 2013] to reduce non-neural variability of the HRF and estimate latent neuronal timeseries. This deconvolution is blind since both HRF and the underlying latent neural timeseries are estimated from only the observed fMRI data. Specifically, we employed the method demonstrated by Wu et al. [2013], which has gained wide usability and acceptance owing to its interpretability, simplicity, robustness, validity and an ever increasing awareness in the community on the importance of deconvolution. Several recent papers have employed it (see for example [Amico et al., 2014; Boly et al., 2015; Lamichhane et al.,

2014]. Briefly, the method models resting-state fMRI data as event-related with randomly occurring events using point processes, and then estimating voxel-specific HRFs using Weiner deconvolution.

Given the high dimensionality of whole-brain fMRI data, mean deconvolved fMRI timeseries were obtained from 125 functionally homogeneous brain regions encompassing the cerebral cortex completely and spread out across it, determined from spectral clustering of resting-state fMRI data (known as the cc200 template [Craddock et al., 2012]. Supporting Information Table S1 provides the names and MNI coordinates of these regions. The template can be downloaded at: http://ccraddock.github.io/cluster_roi/. Further connectivity analysis (performed on Matlab® platform) utilized these 125 timeseries from each participant.

Effective Connectivity Analysis

Whole-brain SEC was obtained using Granger causality (GC) [Deshpande et al., 2010a,b]. GC is an exploratory technique used to quantify directional influences between brain regions. The underlying concept is that, if past values of a timeseries "T1" can, in a mathematical sense, predict the future values of another timeseries "T2," then a causal influence from timeseries T1 to timeseries T2 is inferred [Granger, 1969]. GC employs a multivariate vector autoregressive (MVAR) model to quantitatively predict one timeseries using the other, which is briefly described next.

Given a system defined by k different timeseries $X(t) = [x_1(t), x_2(t), \ldots x_k(t)]$, with k being 125 ROIs in this study, the traditional MVAR model of order p is given by:

$$X(t)=A(1)X(t-1)+A(2)X(t-2)+\cdots+A(p)X(t-p)+E(t) \quad (1)$$

Where $E(t)$ is the model error and $A(1) \ldots A(p)$ are the model coefficients. The coefficients were estimated through multivariate least squares estimation, which calculates the optimal set of coefficients that minimizes the model error in the least squares sense. Model order p must be chosen either by employing a mathematical principle such as the Bayesian Information Criterion (BIC) [Roebroeck et al., 2005] or based on the requirements of the application under consideration. In neuroimaging, the interest is in causal relationships within neural delays of a TR [Deshpande et al., 2013], thus we chose a first order model. Since fMRI's temporal resolution is low, a first order model is shown to capture the most relevant causal information [Deshpande and Hu, 2012].

Coefficient $A(p)$ indicates the degree to which the past $X(t\text{-}p)$ can predict the present $X(t)$. Then, the sum of coefficients of all delays would represent the degree to which all the past values together can predict the present. This formulation is used to evaluate GC by predicting the present value of timeseries-2 (T2) using the past values of timeseries-1 (T1). If, for example, the sum of resulting model coefficients is large, then it implies that T1 can predict T2 very well. If T1's past can predict T2's present, then that implies a causal relationship from T1 to T2. As in previous studies [Kaminski et al., 2001], GC was derived formally, based on the model coefficients, as:

$$GC_{ij}=\sum_{n=1}^{p} a_{ij}(n) \quad (2)$$

Where GC_{ij} is the SEC value from ROI i to ROI j and a_{ij} are the elements of matrix A. It is notable that a single coefficient matrix is obtained for the entire duration of data, and the coefficients do not vary over time. This traditional formulation of GC was slightly modified, as in earlier studies [Deshpande et al., 2010a,b], to remove the effect of zero-lag cross-correlation between timeseries. For this, we included the zero-lag term in Eq.1 as shown below.

$$X(t)=A'(0)X(t)+A'(1)X(t-1)+A'(2)X(t-2)+\cdots +A'(p)X(t-p)+E(t) \quad (3)$$

The diagonal elements of $A(0)$ are set to zero, such that only the instantaneous cross correlation, and not auto correlation, between the timeseries are modeled. The model coefficients obtained from Eq.3 would not be equal to those obtained from Eq.1, since the inclusion of zero-lag term affects other coefficients by removing cross-correlation effects from them. The zero-lag term is thus not used in the evaluation of GC. GC thus obtained would be free from zero-lag correlation effects and is defined as correlation-purged GC (CPGC), which has been widely used in recent times (for example, see [Deshpande et al., 2011, 2015]. A 125 × 125 SEC matrix was obtained for every participant by employing CPGC.

A GC value of 0 represents no causal relationship from the source to the destination region, a value of 1 represents strong positive causality (increase in BOLD response of the source region causes an increase in BOLD response of the destination, and vice versa), and a value of −1 represents strong negative causality (increase in BOLD response of the source region causes decrease in BOLD response of the destination, and vice versa).

Next, DEC was obtained using time-varying dynamic Granger causality (DGC), evaluated in a Kalman filter framework. We employed a dynamic multivariate vector autoregressive (dMVAR) model for estimating DEC [Wheelock et al., 2014; Grant et al., 2014]. The model is "dynamic" because, unlike CPGC formulation, its model coefficients vary as a function of time. Here, DEC is the time-varying physiological process, which is quantified through the DGC measure, which employs the dMVAR model solved in the Kalman filter framework. In DGC, coefficients $A'(p)$ are allowed to vary over time, thus giving coefficients $A'(p,t)$ in the dMVAR model as:

$$X(t)=A'(1,t)X(t-1)+A'(2,t)X(t-2)+\cdots +A'(p,t)X(t-p)+E(t) \quad (4)$$

The dynamic model coefficients are estimated in a Kalman filter framework using variable parameter regression

[Büchel and Friston, 1998]. This involves imposing a forgetting factor, which in our case was chosen to be 1. DGC is then computed as:

$$DGC_{ij}(t) = \sum_{n=1}^{p} a'_{ij}(n,t) \quad (5)$$

Where DGC_{ij}(t) is the DEC value from ROI i to ROI j at a given time point t, and a'_{ij} are the elements of matrix A'. Size of the DEC vector for each connection would be equal to the number of time points in the fMRI data. We compensated for zero-lag cross-correlation effects here also, like in CPGC. Given that our data had 1000 time points, we obtained a 125 × 125 × 1000 DEC matrix for every participant by employing DGC.

Recent simulations [Ryali et al., 2011; Wen et al., 2013] as well as experimental results [David et al., 2008; Katwal et al., 2013; Ryali et al., 2016] suggest that GC applied after deconvolving the HRF from fMRI data (as we have done), is reliable for making inferences about directional influences between brain regions. This method for obtaining SEC and DEC has also been employed in several recent fMRI studies [Bellucci et al., 2017; Deshpande et al., 2013; Feng et al., 2015; Grant et al., 2014, 2015; Hutcheson et al., 2015; Lacey et al., 2014; Sathian et al., 2013; Wheelock et al., 2014]. Variance of DEC (vDEC) was taken as the measure of variability in directional connectivity over time (125 × 125 matrix per participant), which, along with SEC, was used further in identifying disease foci. To comprehend the idea of SEC and DEC from a neuroimaging standpoint, we provide an illustration using a simple example of a pair of real fMRI timeseries (please see Fig. 3).

Identifying Disease Foci

As noted earlier, connectivity modeling identifies interrelationships through connections between brain regions, while our insights on the brain center on functions of regions. Hence, we sought to identify disrupted regional foci in PTSD and PCS + PTSD using EC data.

We used a Bayesian probabilistic model to identify disorder foci from connectivity data [Venkataraman et al., 2013], which assumes that disrupted regions are associated with large number of abnormal connections. The efficacy of this method has been demonstrated earlier with simulations as well as real fMRI data [Zhao et al., 2017], in particular using static functional connectivity (FC) [Venkataraman et al., 2013]. However, their model made certain assumptions on the priors, which were suited for FC data's probability distribution. Here we extend this method to identify disease foci using both static and dynamic EC, albeit with certain modifications in the model formulation given that EC matrices are not symmetric, unlike FC, and that the distributions of FC and EC data are dissimilar. In addition, static and dynamic connectivity data have dissimilar distributions as well. We explain the method briefly before addressing these issues. For a detailed account of the method, please refer to Venkataraman et al. [2013].

The model was originally developed for FC [Venkataraman et al., 2013]. FC measured from fMRI data was seen as a noisy measurement of the unknown latent FC, and was modeled as a Gaussian random variable with the mean and variance dependent on the latent FC. The latent FC was modeled as a tristate variable from a multinomial distribution with three distinct states: positive connection (+1), negative connection (–1) and no connection (0). The model associated the state of each brain region with a binary vector (healthy = 0, disrupted = 1), whose elements followed an independent and identically distributed (i.i.d.) Bernoulli distribution. The model made the following three assumptions: (i) a connection between two disease foci was abnormal with probability 1, (ii) a connection between two nonaffected regions was normal with probability 1, and (iii) a connection between a disease focus and a nonaffected region was abnormal with probability p. The joint likelihood of all the configurations of latent connections between brain regions was modeled as a multinomial distribution model. Upon initiating the model with standard priors (such as the Bernoulli prior for binary state vector, prior for latent FC, etc.), a variational expectation maximization (EM) algorithm was employed [Dempster et al., 1977] for updating the posterior distributions and to solve for the model parameters until they converged. The relative change in free energy of the model by less than 10^{-4} between successive iterations was chosen as the convergence criteria. The model produced posterior probabilities for every region and every connection, using which foci disrupted due to disease and associated connections were identified.

SEC's probability distribution resembled a Gaussian (verified using the Lilliefors normality test), similar to Pearson's correlation. While correlation usually has a distribution with mean ± SD of 0 ± 0.25, SEC's distribution had mean ± SD of 0 ± 0.19, which is acceptable. However, it is not a bounded measure, unlike correlation which is bounded by [–1,1]. The model assumes a tri-state distribution, with default states set to [–1,0,1]. In our entire data, we found a very small number of SEC values that were greater than 1 or smaller than −1 (0.0026%). Hence, we performed inverse Fisher-Z transformation on SEC values to have its distribution bounded by [–1,1]. Similar procedure was followed for vDEC. With both SEC and vDEC, the connectivity matrix is asymmetric, unlike FC, which is a directionless quantity with a symmetric matrix. Hence, the entire matrix was fed into the model, unlike with FC where only the lower or upper triangular part would be used. Put together, these modifications allowed the model to be applied to effective connectivity as well as dynamic connectivity data. Persons interested in the source code (implemented in Matlab©) could contact the corresponding author or Dr. A.V. (archana.venkataraman@jhu.edu).

The Bayesian probabilistic model to determine the foci was evaluated for one thousand times (with different random initiation of priors). Statistical significance of the foci

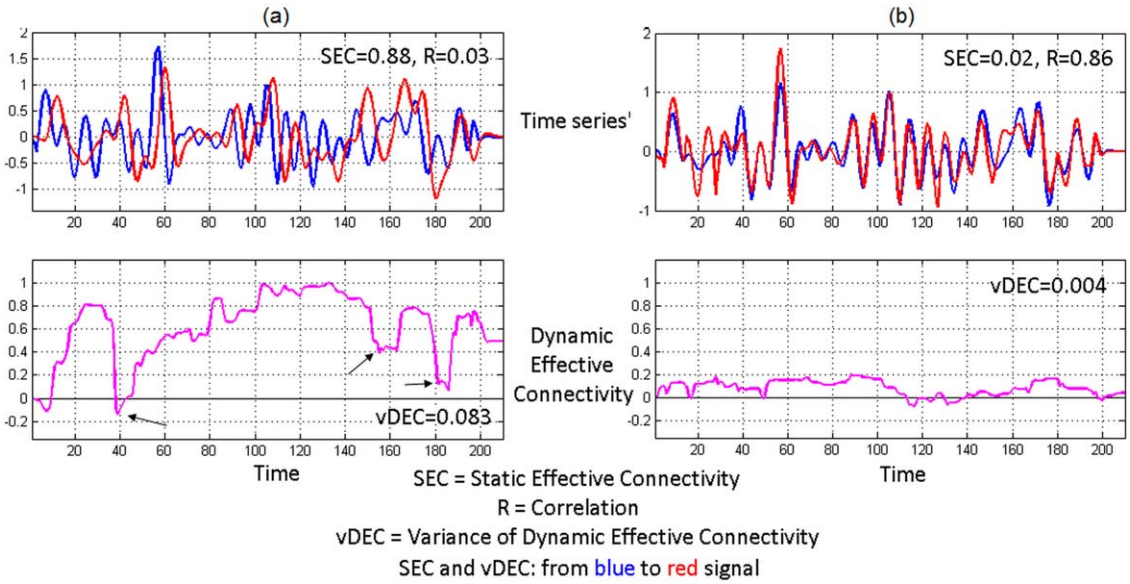

Figure 3.

Illustration of SEC and DEC from a neuroimaging standpoint using two real fMRI time series. In **(a)**, the red timeseries consistently seems to follow after the blue timeseries (top-left figure), indicating that red's associated brain region activates (and deactivates) as soon as blue's region activates (and deactivates), hence a causal influence is inferred and a high SEC value (SEC = 0.88) is observed (note that correlation, which measures zero-lag functional connectivity, is low [$R = 0.03$]). DEC provides further insight (bottom-left figure), which shows that steady causality is maintained mainly in the middle phase, and that causality is lost on three brief instances (where it dips due to observable loss of causality between the timeseries' of those sections [please follow the arrows]). This variability of DEC is quantified in vDEC (vDEC = 0.083). In **(b)**, the two timeseries are nearly overlapping hence highly correlated with $R = 0.86$ (top-right figure). However, the variations in the red timeseries do not occur after (or before) the variations in blue timeseries (and vice versa). This lack of causal relationship results a low SEC value (SEC = 0.02). Correspondingly, DEC (bottom-right figure) lingers around the zero-mark since a causal relationship does not seem to emerge at any point in time. vDEC is also low (vDEC = 0.004). [Color figure can be viewed at wileyonlinelibrary.com]

were determined based on a nonparametric permutation test, as described next. We took the entire dataset and randomly assigned groups. We then fit the model using the standard approach and extracted the posterior probabilities of each region being disrupted by the disease with random group assignment. This was repeated (randomly assigning labels, fitting model, extracting posterior probabilities) for ten thousand iterations to obtain the posterior null distribution for each region. The p-value for each region was then estimated as the proportion of the thousand iterations of model evaluation for which the null posterior (i.e., random assignment) was greater than the foci posterior we had observed when we fit the model with the true labels. We thus obtained significantly affected disease foci in the clinical groups ($P < 0.05$, Bonferroni corrected).

The method also provided affected connectivities associated with the disease foci, which would help in interpreting affected networks from the point of view of the compromised foci. Among such connectivities, we retained only those connections which crossed our statistical significance threshold for effective connectivity values outside of the foci method, in accordance with our primary hypothesis ($P < 0.05$, whole-brain FDR-corrected; controlled for age, education, race and head-motion [using mean frame-wise displacement obtained as defined by Power et al. [2012]. The statistical tests did not control for the comparison of having three groups. This procedure ensured that, irrespective of the model used by us, the significant connections that emerged in this work would have crossed whole-brain multiple comparisons corrected statistical threshold like in most studies, in addition to the fact that the model quantitatively selected these paths using the posteriors. This ensured that our results conformed to multiple layers of verification and statistical standards, in addition to providing novel insights through the foci method.

The model is, in its original form, applicable only for comparison between two groups. Since we were comparing three groups, we overlapped the foci and connections obtained in the three pairwise comparisons to extract only the common foci and connections (intersection). In a

statistical sense, this was the most conservative approach possible. In accordance with our hypothesis, we identified those connectivity paths associated with the compromised foci which exhibited altered SEC (either monotonically reducing or increasing from control to PTSD to comorbid groups) and lower vDEC as we moved from Controls to PTSD to PCS + PTSD. Such a network would disentangle the effects of PTSD as well as comorbid PTSD and PCS, providing novel insights through directional and dynamic connectivity. Results from FC analysis have been reported elsewhere (analysis pipeline is different from what is done in this article) [Rangaprakash et al., 2017a,b,c] and hence we concentrated on directional (or effective) connectivity networks in this report.

Behavioral Relevance of Connectivity Values

To assess the behavioral relevance of connectivity values, we first correlated SEC and vDEC values of each of the identified connectivity paths with symptom severity in PTSD (PCL5 score) and PCS (NSI score), and neurocognitive functioning (NCI score and subtests). Neurocognitive functioning (e.g., cognitive flexibility, executive functioning) is affected in psychiatric disorders such as PTSD and PCS, hence identifying behaviorally relevant connections associated with it carries importance. We report significant correlations, thus associating such connections with altered behaviors.

to get further insight into how the ensemble of identified connections mapped onto the ensemble of behaviors, we performed partial least squares regression (PLSR) analysis [Krishnan et al., 2011]. Using PLSR, we tried to predict symptom severity (PCL5, NSI) and neurocognitive functioning (NCI and subtests) from SEC and vDEC connectivity values of the connections identified from prior analysis. We report the percentage of variance in behaviors explained by the connectivities

Classification Using Support Vector Machine

Statistical separation between neural markers (e.g., a *t*-test) need not necessarily ensure generalizability or predictive ability of those markers for diagnosis [Deshpande et al., 2010a,b]. Statistically significant connectivity paths need not necessarily have high predictive ability and vice versa. Consequently, those connectivities that are both statistically significant (in accordance with our hypothesis) and are top-predictors (high predictive ability) assume superior importance and relevance. We have thus used machine learning approaches to identify such connectivity paths (features) which could accurately classify individuals between controls, PTSD and PCS + PTSD. A Recursive Cluster Elimination based Support Vector Machine (RCE-SVM) classifier [Deshpande et al., 2010a,b] was employed to classify participants based on whole-brain SEC and vDEC values. Notably, findings from prior foci-identification analysis were not used to bias the machine learning algorithm.

First, the data was divided into training data (used to learn patterns in the data) and testing/validation data (used to independently test the learned pattern to assess the quality of the learning). Then, significant group differences were found for all the three comparisons (control vs. PTSD, control vs. PCS + PTSD and PTSD vs. PCS + PTSD) from the training data only, using a threshold of $P < 0.05$ (controlled for age, race, education and head motion) for both SEC and vDEC, and an uncorrected $P < 0.05$ threshold was used since we wanted to be liberal about which features are fed into the classifier, thus letting the classifier choose the most predictive features. We next found overlapping connectivity paths between the three comparisons. The resulting SEC and vDEC features were combined to provide the input features to the classifier. This initial filtering is known to enhance the quality of classification [Craddock et al., 2009] by ensuring that nondiscriminatory features are not input into the classifier.

Our choice of support vector machine (SVM) [Vapnik, 1995] for classification was driven by its wide applicability and acceptance for classification in several fields, including neuroimaging [Wang, 2005]. Prior studies showed that the use of discriminatory features enhances classification performance of SVMs [Craddock et al., 2009; Deshpande et al., 2010a,b]. We thus employed recursive cluster elimination (RCE), a wrapper method, which iteratively eliminates features to minimize prediction error, wherein feature selection and classification steps are embedded together. The RCE-SVM classification technique involves the clustering step, the SVM scoring step and the RCE step. Features that were initially fed into the classifier were divided into training and testing datasets. The classifier was trained using the training data, while the testing data was totally kept blinded to the classifier. Once training was complete, the testing data was fed into the classifier and classification accuracy was obtained. This ensured generalizability of the results.

In the clustering step, k-means algorithm was employed to cluster the training data into "n" clusters. The "n" obtained through this iteration served as the initial "n" for the RCE-SVM loop. The initial number of clusters were the number of clusters into which the k-means algorithm would cluster the input connectivity features. Choosing smaller number of clusters would assign more number of features to each cluster, thus eliminating more features in each successive recursive cluster elimination (RCE) step. Though this may speed up the execution, it would leave fewer good features as the RCE steps advance towards the end, which may reduce the classification accuracy. Choosing larger number of clusters would assign smaller number of features to each cluster, which would increase the execution time. Assessing this tradeoff, prior studies [Deshpande et al., 2010a,b] have recommended using about 40 initial number of clusters. We used the value of 40 in this study. In the SVM-scoring step, each cluster was

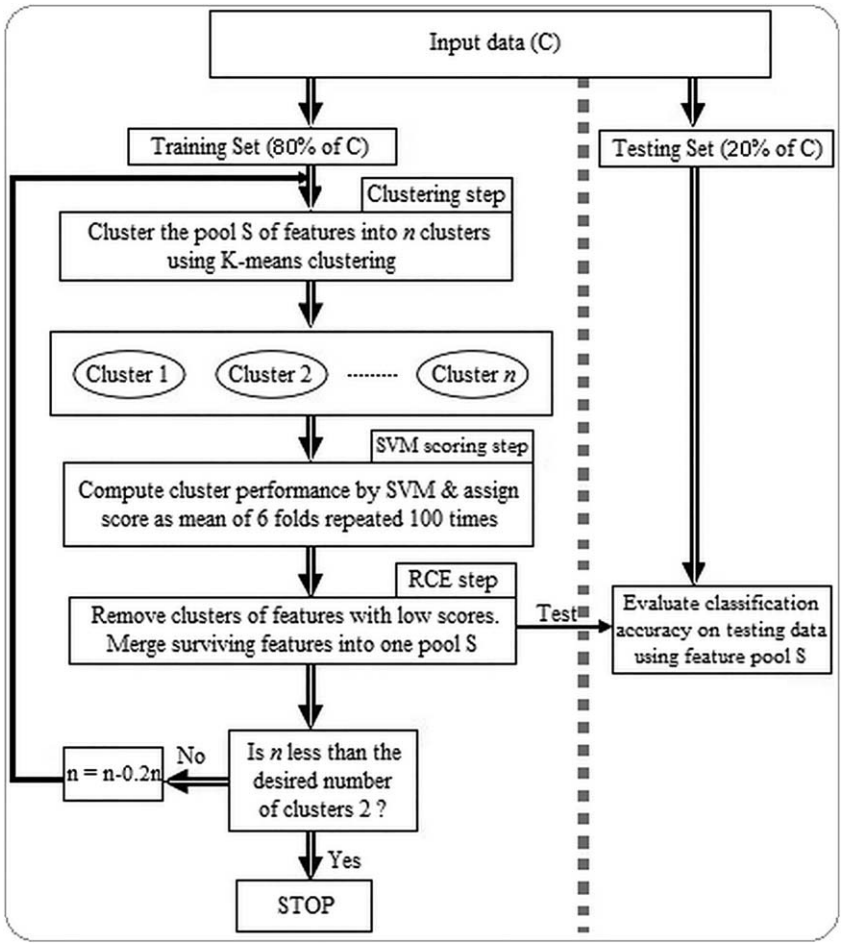

Figure 4.
Flowchart illustrating the recursive cluster elimination based support vector machine (RCE-SVM) classification procedure.

scored based on its ability to differentiate between the groups by employing linear SVM. To assess the performance of clusters, the training data was randomly partitioned into six nonoverlapping subsets of equal sizes (six folds). The SVM was trained using 5 of the 6 subsets. Performance (accuracy) was calculated using the remaining subset. As such, given that we had 174 fMRI scans, each iteration included the training data of 174*5/6 (=145) randomly chosen from each group ($5/6^{th}$ of each group), and the remaining 29 as the testing data. All possible partitions were generated by repeating the clustering and cross-validation procedures hundred times. Such independent repetitions have no theoretical limits and no stopping criteria, and we chose to repeat it 100 times based on previous reports [Deshpande et al., 2010a,b] that found that 100 repetitions are sufficient to reliably estimate the classification accuracy. For each of these hundred repetitions, classification accuracy was obtained using the testing data.

Utilizing the outcome of hundred repetitions and six folds for each repetition, the average accuracy was assigned as the cluster's score. The bottom 20% of low scoring clusters were discarded in the RCE step. The remaining features were merged and the value of "*n*" was reduced by 20%. This ensured that only certain top classifying features qualified for the next iteration. The clustering step, the SVM-scoring step and the RCE step were again iteratively repeated. After each iteration, performance of the classifier was computed using the reduced number of features compared to the earlier iterations. Once the number of clusters reached two, the procedure was terminated. Figure 4 illustrates the RCE-SVM procedure through a flowchart. Complete separation of training and testing datasets eliminates bias in the evaluation of classification accuracy [Kriegeskorte et al., 2009]. Further, the features obtained in the final two clusters would be those with highest discriminative ability and hence carry predictive value for diagnosis. Complete details of the RCE-SVM algorithm can be obtained from previous reports [Deshpande et al., 2010a,b; Yousef et al., 2007].

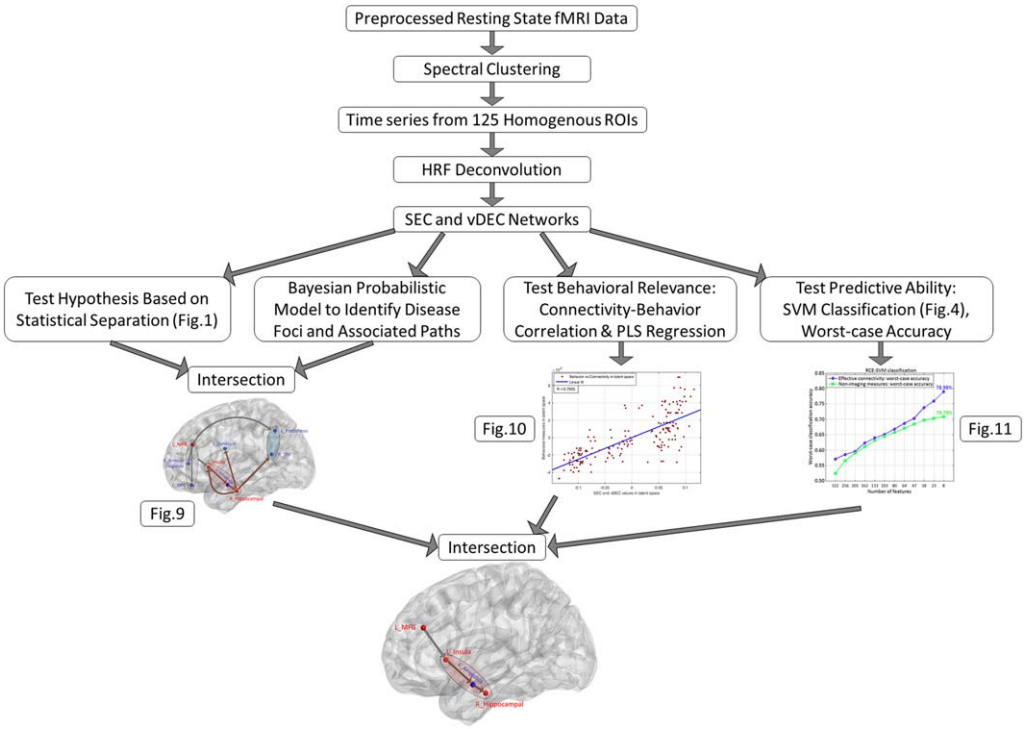

Figure 5.
Schematic of the entire processing pipeline employed in this work. [Color figure can be viewed at wileyonlinelibrary.com]

In this study, the following parameter choices were made. 80% of the participants were marked as the training set, with 20% being marked as the testing set. We started the algorithm with 40 clusters in the first RCE step. The bottom 20% of clusters (based on performance) were eliminated in each of the subsequent RCE steps. The final RCE step consisted of two clusters containing the top-predictive features. Over 100 random iterations, six-fold cross validation was performed, resulting in an aggregate of 600 iterations over the entire execution.

To be conservative, we evaluated the worst-case classification accuracy by considering the least accuracy value obtained from the test data among all 600 iterations (100 repetitions $\times$ 6 folds). Statistical significance of accuracies was obtained by estimating p-values using a binomial null distribution $B(\eta,\rho)$, η being the number of participants and ρ being the probability of accurate classification, as in previous studies [Pereira et al., 2009]. Only those accuracies with p-values less than 0.05 (Bonferroni corrected) were considered as statistically significant for reporting. The Bonferroni p-value threshold was determined as 0.05 divided by: (number of groups $\times$ number of clusters).

Machine learning classification was utilized in this work to serve two purposes: (i) determine predictive ability of the features, and (ii) identify top predictive features. While we primarily performed this with connectivity features, we wanted to compare our findings against those measures that are more commonly used clinically today. Hence we chose to perform classification with the nonimaging measures. We predicted that that connectivity will better predict the diagnostic membership of a novel subject than the available nonimaging measures, given that connectivity features are derived from brain data. We repeated the aforementioned procedure to perform classification independently by using 32 available nonimaging measures as input features instead of SEC and vDEC features. The 32 measures were: (i) behavioral measures: all CNS-VS measures including the NCI score; (ii) exposure/injury descriptives: Combat Exposure Scale, lifetime concussions and Life Events Checklist (iii) psychological health measures: Perceived Stress Scale, Pittsburgh Sleep Quality Index, Epworth Sleepiness Scale, Zung Anxiety Scale, and Zung Depression Scale. Worst-case classification accuracies and top-classifying features were obtained, and these were compared with the results obtained using connectivities. In Figure 5, we have summarized the processing pipeline of all methods used.

RESULTS

Demographics

Demographics for the three groups are presented in Table I. There were no significant differences between the groups in age, $P = 0.699$, or education, $P = 0.152$. Results indicated that there was a difference in the frequency of

TABLE I. Basic demographics

Variable		Controls	PTSD	PCS + PTSD
Age, years	Mean	32.6	32.2	33.7
	Median	31	32	33
	SD	6.7	7.6	6.8
	Range	24	24	30
Education, years	Mean	15.1	14.5	14.1
	Median	16	14	14
	SD	1.9	2.2	1.9
	Range	8	9	8
Race	White	18 (66.7%)	11 (64.7%)	26 (66.7%)
	Black	2 (7.4%)	3 (17.6%)	9 (22.0%)
	Hispanic	3 (11.1%)	3 (17.6%)	2 (4.9%)
	Asian	2 (7.4%)	0	1 (2.4%)
	Other	0	0	1 (2.4%)
Medication		2 (7.4%)	4 (23.5%)	13 (31.7%)[a]
Lifetime mTBIs	Mean (Range)	0.3 (2)	1.1 (6)	2.5 (15)[a]

[a]Statistically significant (corrected $P < 0.05$), Controls vs. PCS + PTSD.

reported psychotropic use between groups, $\tau b = 0.24$, $P = 0.011$, with the comorbid group having highest percentage of medicated participants. There was significant difference between groups in the number of reported lifetime mTBIs, $F(2, 171) = 5.81$, $P = 0.004$, specifically between control and PCS + PTSD groups, but not the PTSD and PCS + PTSD groups or control and PTSD groups, $P > 0.05$.

Psychological Health and Neurocognitive Function

Results revealed statistically significant differences between all three groups in posttraumatic symptoms (PCL5), $F(2, 81) = 101.65$, $P < 0.001$, postconcussive symptoms (NSI), $F(2, 78) = 49.79$, $P < 0.001$, and combat exposure (CES), $F(2, 79) = 40.69$, $P < 0.001$. All P-values retained significance after multiple comparisons correction. As observed in Table II, the PCS + PTSD group had the highest scores out of the three groups on these measures.

Results indicated that after multiple comparisons correction, the control group had significantly higher scores than PCS + PTSD group on all neurocognitive measures, $P < 0.05$, with the exception of Verbal Memory and Reaction Time, $P > 0.05$. PCS + PTSD group also had significantly lower scores in Cognitive Flexibility, Executive Functioning, and the NCI compared to PTSD group, $P < 0.05$. The findings suggest that both PTSD and PCS + PTSD groups have lower scores than controls, but also that the comorbid group has greater impairments than the PTSD group (see Table II).

FMRI Connectivity Results

We evaluated SEC and vDEC from resting-state fMRI data, and used that in a novel framework to identify disrupted regional foci and their associated disrupted connections in the clinical groups in accordance with our hypothesis. We identified three foci: (i) left middle frontal gyrus (MFG), which mainly included parts of BA9 and BA10, which overlaps with the dorsolateral prefrontal cortex (DLPFC) (ii) left anterior insula, and (iii) right hippocampal formation (included anterior parts of hippocampus, parahippocampal gyrus, entorhinal and perirhinal cortices). These affected foci were connected to/from other brain regions that were part of the disrupted network (see Fig. 6 for the affected ROIs and Table III for the affected connections with MNI coordinates).

Figure 7 shows the networks associated with each focus. It shows widespread dysregulation originating from the MFG (Fig. 7a), information from frontal and hippocampal regions relayed to the amygdala via the insula (Fig. 7b),

TABLE II. Mean, median, and standard deviation on PCL5, NSI, CES, and CNS-VS neurocognitive measures for each of the groups

		Controls	PTSD	PCS + PTSD
Psychological				
Traumatic stress[a] (PCL5 score)	Mean	23.5	56.6	70.9
	Median	21.5	48.5	70.5
	SD	4.2	17.8	15.2
Postconcussive Symptoms[a] (NSI score)	Mean	6.6	25.9	43.4
	Median	5	17.5	41.5
	SD	4.8	19.2	16.1
Combat exposure[a]	Mean	7.2	16.7	28.6
	Median	2.5	15	29
	SD	9.8	11.2	8.6
Neurocognitive				
Neurocognitive Composite index[b]	Mean	101.2	94.3	81.7
	Median	100.7	94.6	82.2
	SD	12.9	12.5	20.7
Reaction time	Mean	97.4	95.3	84
	Median	101	92	91
	SD	23	11.9	32.8
Complex attention[c]	Mean	94.2	78.1	70
	Median	99.5	92	80
	SD	23.3	30.9	31.3
Cognitive flexibility[b]	Mean	103.6	97.1	80.5
	Median	103	93	86
	SD	16.3	15.2	26.7
Processing speed[c]	Mean	104.8	100.1	89.9
	Median	104	98	92
	SD	20.9	11	20.1
Executive functioning[b]	Mean	106	101	84.1
	Median	104.5	104	90
	SD	13.3	13.2	24.8
Verbal memory	Mean	99.6	92.1	83.6
	Median	106.5	103	83
	SD	12.5	9.5	13.9

[a]Denotes $P < .05$, all three groups.
[b]Denotes $P < .05$, PCS + PTSD vs. Control and PTSD groups.
[c]Denotes $P < .05$, PCS + PTSD vs. Controls.
Note: Traumatic Stress = PCL5; Postconcussive Symptoms = NSI; Combat Exposure = CES.

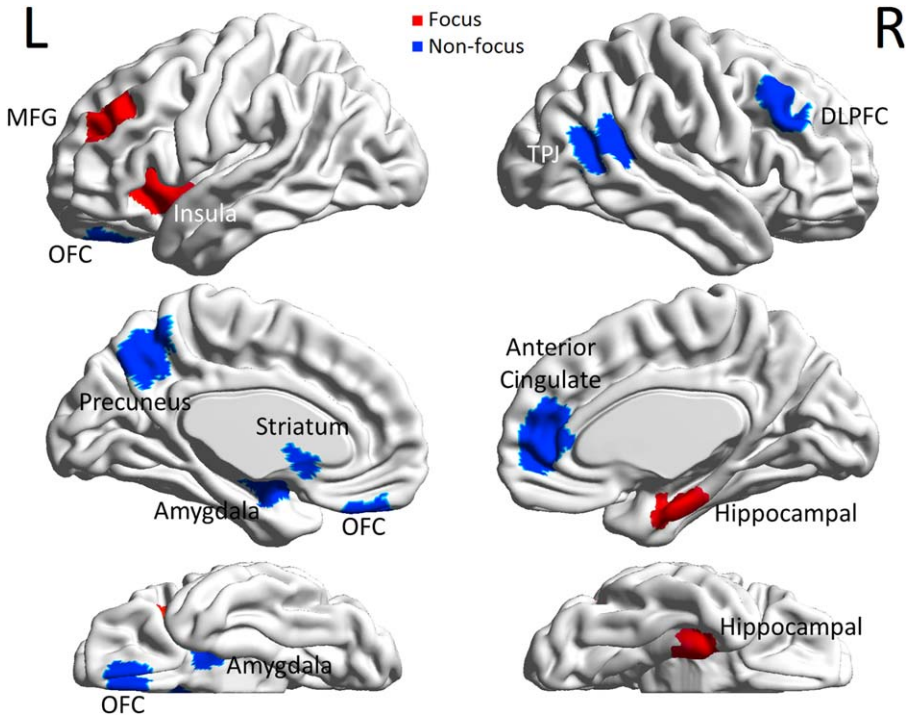

Figure 6.

Brain regions (with exact region boundaries) involved in the affected network. The regions were defined based on the cc200 functional brain atlas (Craddock et al., 2012). Regions in red are the affected foci and those in blue are the regions connected to/from the affected foci. MFG = middle frontal gyrus, OFC = orbito-frontal cortex, TPJ-temporo-parietal junction, DLPFC = dorsolateral prefrontal cortex. This visualization was performed using BrainNet Viewer (Xia et al., 2013). [Color figure can be viewed at wileyonlinelibrary.com]

followed by an overdrive of memory-related regions driven by the hippocampus (Fig. 7c). Further clarity was obtained by splitting the network into three, based on dominant functionality (Fig. 8): (i) prefrontal top-down dysregulation network, with disruption originating from the MFG, causing direct and indirect (through OFC and

TABLE III. The 12 paths whose effective connectivity values were found to be significantly different between the three groups, in accordance with our hypothesis

		MNI coordinates of centroid (x, y, z)	
Path no.	Path	Source	Destination
1	L_MFG → L_Insula	−31.4, 39.1, 28.3	−32.9, 20.5, 1.9
2	L_Insula → L_Amygdala	−32.9, 20.5, 1.9	−23.1, −2.6, −20.5
3	L_Amyg → R_Hippocampus	−23.1, −2.6, −20.5	19.4, −12.4, −25.5
4	L_MFG → L_OFC	−31.4, 39.1, 28.3	−8.1, 40.3, −28.9
5	L_OFC → L_Insula	−8.1, 40.3, −28.9	−32.9, 20.5, 1.9
6	L_MFG → R_Ant_Cingulate	−31.4, 39.1, 28.3	10.3, 44.2, 6.5
7	R_Ant_Cingulate → L_Insula	10.3, 44.2, 6.5	−32.9, 20.5, 1.9
8	R_Hippocampus → L_Insula	19.4, −12.4, −25.5	−32.9, 20.5, 1.9
9	R_Hippocampus → L_Precuneus	19.4, −12.4, −25.5	1.23, −57.1, 44.6
10	R_Hippocampus → L_Striatum	19.4, −12.4, −25.5	−11.3, 12.2, 3.5
11	L_MFG → R_TPJ	−31.4, 39.1, 28.3	46.3, −53.4, 16.9
12	L_MFG → R_DLPFC	−31.4, 39.1, 28.3	47.1, 26.6, 37.1

Table provides the Montreal Neurological Institute (MNI) coordinates for the centroids of the brain regions associated with these connectivity paths. MFG = middle frontal gyrus, OFC = orbito-frontal cortex, TPJ = temporo-parietal junction, DLPFC = dorsolateral prefrontal cortex.

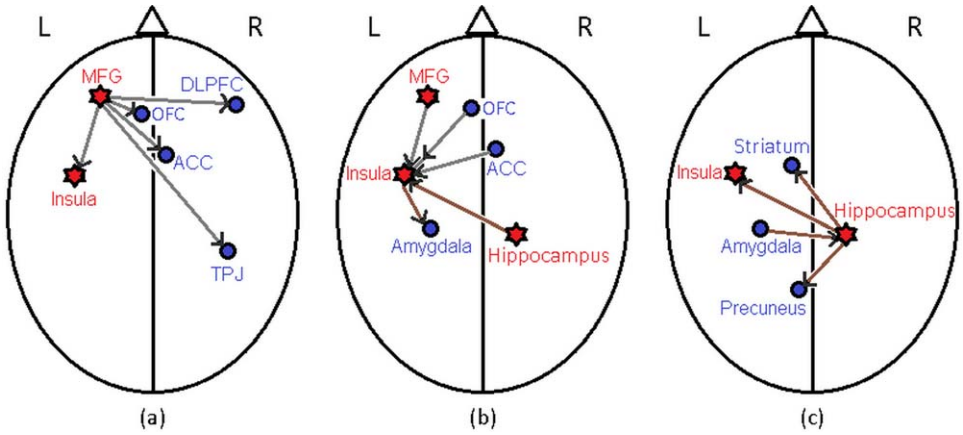

Figure 7.

Breakup of the identified disrupted network into three networks associated with the following three identified foci (in red stars): **(a)** left middle frontal gyrus (MFG) focus, showing widespread dysregulation originating from this region, **(b)** left anterior insula focus, which integrates information from prefrontal and hippocampal regions, and relays it to the amygdala, and **(c)** right hippocampal formation focus, which relays subcortical overdrive to the regions associated with memory processing. Gray lines correspond to those connections with lower SEC (dysregulation); brown lines correspond to those connections with higher SEC (overdrive). All paths followed this trend with vDEC: PCS + PTSD < PTSD < Controls. [Color figure can be viewed at wileyonlinelibrary.com]

ACC) dysregulation of the insula as well as temporo-parietal junction (TPJ), (ii) insula → amygdala → hippocampal loop of elevated connectivity which, considering as a graph of connected nodes, appears to be in a "positive-feedback" loop representing under-restrained subcortical overdrive [Cerullo et al., 2012], caused due to frontal disinhibition mediated by the insula, and (iii) hippocampal memory-related network which likely translates and mediates the subcortical overdrive into elevated retrieval of traumatic memories through overdrive of association areas

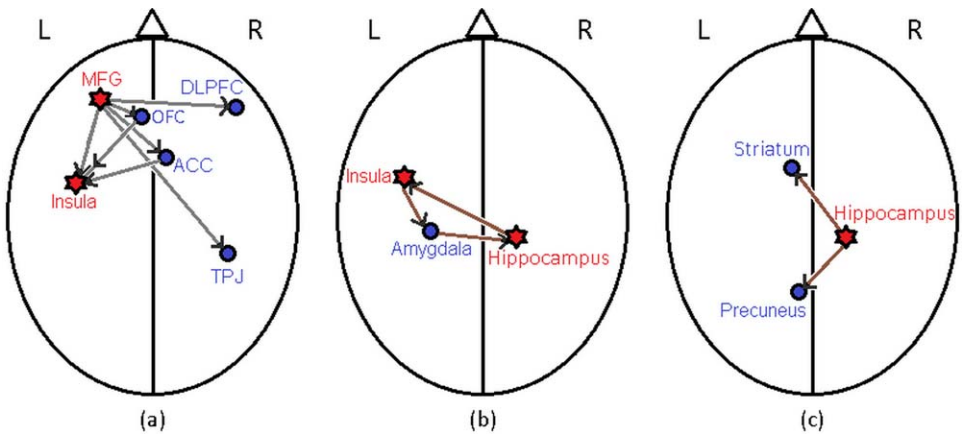

Figure 8.

Breakup of the identified network into three networks associated with generally three different functions: **(a)** prefrontal top-down dysregulation network, with disruption originating from the MFG, causing direct and indirect (via other regions) influence on the insula and temporo-parietal junction (TPJ), **(b)** insula → amygdala → hippocampal loop, which is likely a "positive-feedback" loop representing under-restrained subcortical overdrive, and **(c)** hippocampal memory-related network, which likely mediates and translates the subcortical overdrive into elevated retrieval of traumatic memories, leading to documented PTSD symptoms like trauma re-experiencing, hyperarousal and flashbacks. Gray lines correspond to connections with lower SEC (dysregulation) and brown lines correspond to connections with higher SEC (overdrive). Foci are in red, non-foci are in blue. [Color figure can be viewed at wileyonlinelibrary.com]

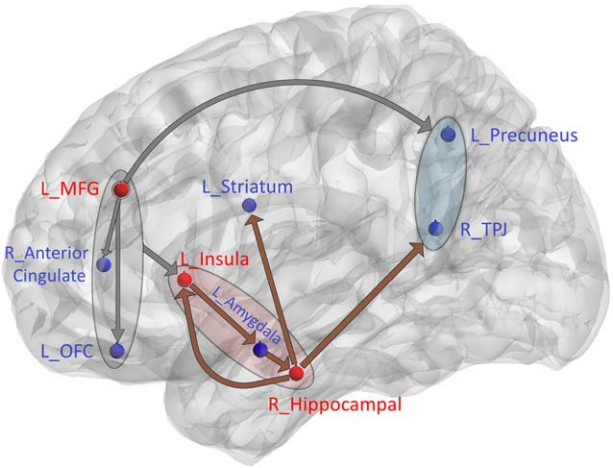

Figure 9.

The disrupted foci and the disrupted connections associated with the foci as a possible mechanistic model of neural aberrations in PTSD and PCS: The prefrontal regions, with the left MFG as the driver, are impaired in their ability to regulate the left insula, which does not inhibit the subcortical regions adequately, resulting in overdrive. This subcortical overdrive would cause elevated emotion and memory processing, culminating in overdriven parietal memory-related regions, which would result in the elevated behavioral manifestations often observed in soldiers with PTSD and PCS. Gray lines correspond to connections with lower SEC (dysregulation); brown lines correspond to connections with higher SEC (overdrive); and all paths exhibited lower vDEC (lower flexibility) in the clinical groups compared to controls (with the trend PCS + PTSD < PTSD < Controls). Foci are in red, nonfoci are in blue. This visualization was performed using BrainNet Viewer (Xia et al., 2013). [Color figure can be viewed at wileyonlinelibrary.com]

involving memory processing/retrieval. This likely leads to re-experiencing traumatic events, hyperarousal, flashbacks and other symptoms often observed in PTSD.

Taken collectively, we identified the MFG to be the pivotal source of network disruption in soldiers with PTSD and PTSD with comorbid PCS (Fig. 9), which further resulted in network disruption across other emotion and memory related regions, potentially exacerbating symptoms. This network provides a mechanistic explanation of the emotion dysregulation circuitry, which subsequently results in the reoccurrence of traumatic memories associated with PTSD.

Behavioral Relevance of Connectivity Values

Connectivity values of three paths (paths 1–3 in Table III) had significant association with neurocognitive functioning (neurocognitive-composite-index [NCI] and subtests), PTSD symptoms (PCL5-score) and PCS severity (NSI-score) (see Table IV), thus highlighting their relevance to the underlying neuropathology. The remaining significant connectivity paths were not strongly associated with these behaviors, hence did not cross the significance threshold ($p < 10^{-20}$, Bonferroni's correction). It was notable that the associations followed the expected trend: increase in symptom severity (PCL5, NSI) and decrease in behavioral performance (NCI) corresponded to higher SEC in the overdrive paths (L_Insula → L_Amygdala and L_Amyg → R_Hippocampus), lower SEC in dysregulation paths (L_MFG → L_Insula), and lower vDEC in all paths. In other words, worse behaviors corresponded with worse connectivities as defined by our hypothesis. Demographics (age, education) did not have any significant association with any of the results.

Several of the 12 connections exhibited significant associations with several of the behaviors (75.5% of the associations were significant with $P < 0.05$). This suggests that the 12 connectivities, taken together, might be more behaviorally relevant than the individual connectivities themselves. Therefore, we performed partial least squares regression (PLSR) to evaluate the combined ability of the 12 connections to predict the combined set of 9 behaviors (PCL5 and NSI scores, NCI and its 6 subtests). We found that SEC values could explain 47.25% variance in the behaviors, while vDEC could explain 48.29% variance.

TABLE IV. Association of SEC and vDEC values of the three pivotal connectivity paths with the NCI score and symptom severity in PTSD (PCL5 score) and PCS (NSI score)

	Symptom severity score		Behavioral measure
Path	PCL5 score (PTSD)	NSI score (PCS)	Neurocognitive composite index (NCI)
SEC			
L_MFG → L_Insula	−0.6852	−0.6780	0.6229
L_Insula → L_Amygdala	0.6650	0.6816	−0.5945
L_Amyg → R_Hippocampus	0.7203	0.7022	−0.6642
vDEC			
L_MFG → L_Insula	−0.6462	−0.6544	0.6507
L_Insula → L_Amygdala	−0.6728	−0.6805	0.6462
L_Amyg → R_Hippocampus	−0.6896	−0.6981	0.6534

Table presents the correlation values (*R*-value), which were significant with Bonferroni-corrected *P*-values smaller than 10^{-20}.

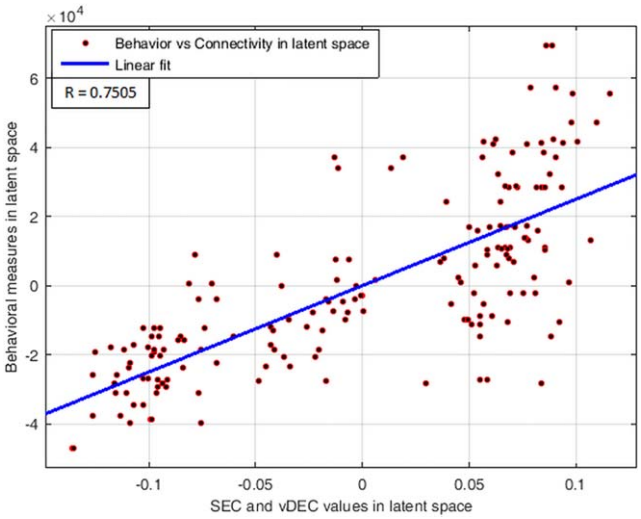

Figure 10.

Partial least squares regression maps the independent (all significant connectivity combined) and dependent (all behaviors combined) variables into a latent space and finds an aggregate relationship between them through it. The latent space, in which the regression presented in the figure is performed, contains categorical variables which holds an aggregate of all significant connectivities (which fit our hypothesis) and all behaviors, so that their correlation in the latent space could be considered as the net association of all the connectivities with all the behaviors. Figure shows the linear fit between significant SEC as well as vDEC connectivity values (the 12 paths presented in Table III) with behaviors (PCL5, NSI, NCI and subtests) in the latent space ($R = 0.75$, $P = 9.3 \times 10^{-33}$). [Color figure can be viewed at wileyonlinelibrary.com]

When combined SEC and vDEC values were taken, they could explain 57.08% variance in the behaviors. A strong association between connectivities and behaviors ($R = 0.75$, $P = 9.3 \times 10^{-33}$) was found in the latent space (see Fig. 10 for linear fit). The latent space contains categorical variables that represent all connectivities and behaviors included in the model in an abstract form, so that their correlation in the latent space could be considered as the net association of all the connectivities with all the behaviors. Our finding reiterates the fact that the 12 connectivity paths identified in this work are, taken together, behaviorally relevant.

Machine Learning Classification Results

In simple terms, statistical significance implies that the difference in population mean values of the metric (e.g., connectivity) is large in relative comparison to the population standard deviations. It implies that it is safe to infer, with certain confidence, that a difference of significance is exhibited by the two populations. However, success in such hypothesis testing is neither necessary nor sufficient to assure that the diagnostic membership of a novel subject based on a novel measurement can be predicted by the measure. A mechanism for quantifying the predictive ability of the features is not provided by hypothesis testing, underscoring the importance of acknowledging what a technique like hypothesis testing could do, and could not do.

Statistically significant neural signatures need not necessarily possess generalizability or predictive ability, implying that connectivities that are statistically significant, conforming to our hypothesis and at the same time are also top predictors of the diagnostic label assume higher importance. Top predictors are those connectivities that, among all connectivities, possess the highest ability in predicting the diagnostic membership of a novel subject. We thus employed recursive cluster elimination based support vector machine (RCE-SVM) classifier [Deshpande et al., 2010a,b] to identify the top predictors. As elucidated earlier, it eliminates low-performing connectivity features recursively, finally identifying those features that contribute towards obtaining highest classification accuracy. Machine learning classification techniques such as RCE-SVM learn the underlying patterns in the training data set, and apply the learned pattern on an untouched testing data set, finally classifying the "test" participants into one of the groups. The classification accuracy measures how good the classification was performed using the features we provided to the classifier.

Classification was performed for two different paradigms: (i) classification using 32 nonimaging measures (NIMs), and (ii) classification using connectivities from the entire brain (complete data, nothing left behind). We found that classification using connectivities provided significantly higher accuracy (about 8% more, $P < 0.05$ Bonferroni-corrected) than classification using NIMs (see Fig. 11). This finding indicates that SEC and vDEC have better predictive ability in identifying subjects with PTSD and PCS compared to NIMs.

Table V summarizes worst-case classification accuracies along with top-predictive features (see Fig. 12 for average accuracy). Along with classification accuracies, the top-predictors that resulted in the highest classification accuracy are also of considerable interest. For classification using connectivities, SEC and vDEC values of four connectivity paths were the top-predictive features (L_MFG→L_Insula, L_Insula→L_Amygdala, L_Amygdala→R_Hippocampus and R_Ant_Cingulate→R_Inferior_Frontal). The first three connectivity paths were among the twelve paths to have emerged significant in this study (paths 1–3 in Table III), which also had significant associations with symptom severity and neurocognitive functioning. Prior to these findings, these connectivity paths were attributed only with statistical significance between groups and behavioral relevance. Statistical significance does not necessarily guarantee predictive ability of connectivity features [Pereira et al., 2009]. These results show that, in addition to statistical separation and behavioral relevance, these connectivity paths also

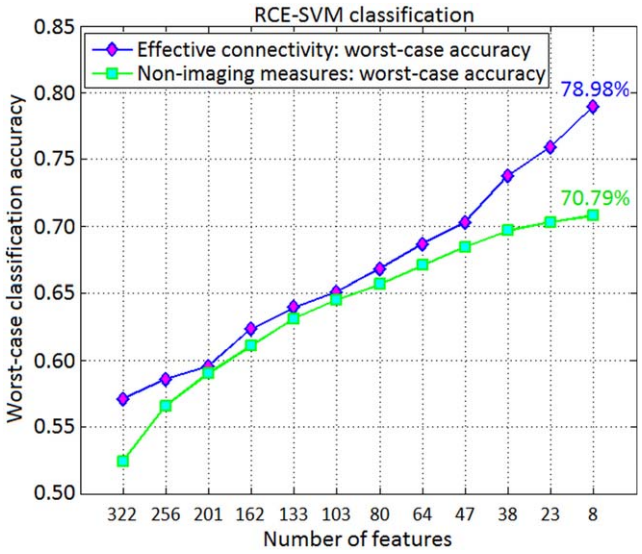

Figure 11.

Machine learning classification was performed using recursive cluster elimination based support vector machine (RCE-SVM) classifier, to classify between PTSD, PCS + PTSD and control groups. Figure shows worst-case classification accuracies obtained using recursively reducing number of discriminative features (poorer features are successively eliminated). Classification was performed independently with both whole-brain effective connectivity values and nonimaging measures (NIMs). We observed that connectivities consistently outperformed NIMs, with 8% better performance in the final RCE step using top-predictive connectivity features. [Color figure can be viewed at wileyonlinelibrary.com]

possess the highest predictive ability, all obtained in a data-driven way from whole-brain connectivity data. Figure 5 summarizes the processing pipeline of our entire work, along with the corresponding results.

DISCUSSION

In the current study, we sought to identify the foci of network disruption from effective connectivity networks in soldiers with PTSD and PCS. We hypothesized that these disorders are associated with compromised foci, which are in turn associated with compromised connections that have altered SEC and lower vDEC in the clinical groups. We found evidence in favor of our hypothesis. Our findings revealed three compromised foci (L_MFG, L_Insula and R_Hippocampus) which were significantly different between all three groups in accordance with our hypothesis. Our results also revealed a network of affected connections in accordance with our hypothesis (Fig. 9). The results showed widespread dysregulation originating from the MFG. We found that the prefrontal regions, steered by the MFG, exhibited reduced influence on the insula in the clinical groups, which was mediated by the OFC and ACC. This resulted in insular disinhibition of the amygdala and hippocampus, which might contribute to an overdrive of these sub-cortical regions. This overdrive subsequently manifested through disinhibited parietal (TPJ, precuneus) and other subcortical regions (striatum), which would ultimately result in elevated behaviors often observed in these disorders. The network was obtained from resting-state data, hence represents the differences in baseline state between the groups. Based on prior knowledge underpinning the neural mechanisms of cognitive emotion regulation [Gross, 2014], we propose that this network (Fig. 9) represents prefrontal dysregulation of emotion, leading to inadequate control over highly arousing traumatic memories, which gives rise to trauma re-experiencing, hyperarousal, flashbacks and other symptoms commonly observed in soldiers with PTSD and comorbid PCS + PTSD. This is the first fMRI study to have investigated effective connectivity in either PTSD or mTBI or the comorbid condition.

The MFG is known to play a key role in cognitive control [Emmert et al., 2016], which includes top-down regulation of emotions. Although the amygdala is key to emotion generation, and medial prefrontal regions primarily mediate subconscious emotion regulation such as fear conditioning [Gross, 2014], lateral prefrontal regions (e.g., MFG) are responsible for the initiation of voluntary cognitive regulation of emotion [Gross, 2014]. Several studies have speculated that the MFG could be the likely source of network disruption in PTSD [Kennis et al., 2015; White

TABLE V. Machine learning classification was performed using recursive cluster elimination based support vector machine (RCE-SVM), to classify between PTSD, PCS + PTSD and control groups

	Worst-case accuracy	Top-predictive features
Nonimaging measures	70.79%	Epworth sleepiness scale and Zung depression scale
Connectivity values	78.98%	SEC and vDEC of paths 1–3 (see Table III) and R_Ant_Cingulate -> R_Inf_Frontal
P-value for row-wise comparison	4.48×10^{-24}	

Table presents the obtained worst-case classification accuracies along with the top-predictive features responsible for resulting in this accuracy.

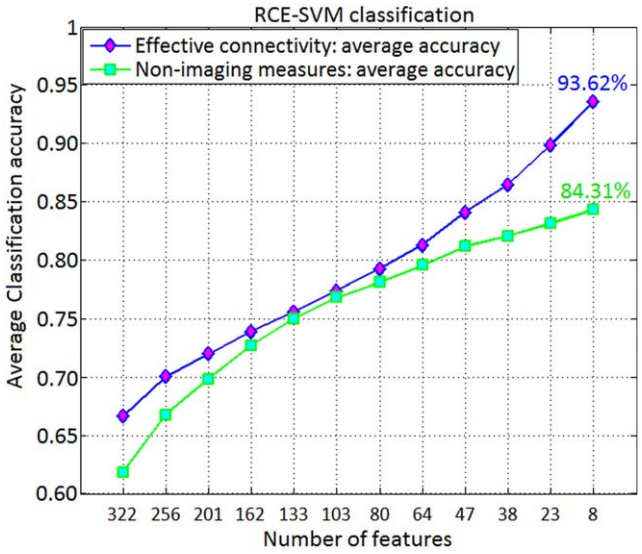

Figure 12.

Machine learning classification was performed using recursive cluster elimination based support vector machine (RCE-SVM) classifier, to classify between PTSD, PCS + PTSD and control groups. Figure shows average classification accuracies obtained using recursively reducing number of discriminative features (poorer features are successively eliminated). Classification was performed independently with both whole-brain effective connectivity values and nonimaging measures (NIMs). We observed that connectivities consistently outperformed NIMs, with 9% better performance in the final RCE step using top-predictive connectivity features. The trend is highly similar to what was observed with worst-case accuracies. [Color figure can be viewed at wileyonlinelibrary.com]

et al., 2014], including a recent meta-analysis [Simmons and Matthews, 2012]; although direct evidence for this hypothesis had not emerged so far. We provide evidence, what we believe to be the first of such evidence for their hypotheses. In support of this interpretation of our findings, a recent meta-analysis discussing evidences from several papers concluded that repetitive transcranial magnetic stimulation (rTMS) applied to the MFG could be used as a treatment for PTSD [Berlim and Van Den Eynde, 2014]. While that paper does not posit the underlying mechanism, we provide evidence for the network of disturbance resulting from MFG dysfunction, with MFG as the source of the network disruption. As such, MFG's role is the initiation of cognitive control, including emotion regulation, whose disruption could thus lead to a chain reaction of impaired cognitive control or emotion dysregulation.

In addition to the aforementioned, we observed prefrontal, top-down dysregulation of the insula by the MFG (both direct and indirect via OFC and ACC). The OFC is considered important for social emotional processing as well as emotion regulation execution [Gross, 2014]. The ACC plays the key role of executive functioning in cognitive control [Gross, 2014]. Together, the OFC and ACC appear to represent an executive arm of cognitive control, which when insufficiently driven by MFG, could directly contribute to the dysregulation other regions such as insula.

The anterior insula is largely involved in mediating between the prefrontal cortex and subcortical regions, and is found to be implicated in emotion dysregulation [Gross, 2014; Thayer and Lane, 2000]. It is substantially connected to the amygdala through white-matter tracts [Oishi et al., 2015], and plays a vital role in subjective emotional experience (feelings) [Rolls et al., 2008]. It is implicated in the integration of emotionally relevant information from multiple sources in the brain, representing them as of one of the several complex emotions [Alba-Ferrara et al., 2011]. In our findings, prefrontal dysregulation of the insula likely leads to its elevated engagement with (or the overdrive of) the amygdala, which in effect causes overdrive of the hippocampus. Specifically, connections *from* the prefrontal cortex *to* the insula exhibited reduced connectivity. Based on prior knowledge on the relationship between the prefrontal cortex, insula and subcortex [Gross, 2014], reduced connectivity from the prefrontal cortex to the insula corresponds to lower prefrontal top-down modulation, and elevated connectivity among the insula, amygdala and hippocampus corresponds to pathologically enhanced engagement or an "overdrive."

Overdrive of hippocampus, a key region involved in declarative memories [Squire and Wixted, 2011], could indicate elevated retrieval of explicit traumatic memories. The critical role of amygdala and hippocampus in PTSD and PCS have been well documented [Costanzo et al., 2014; Simmons and Matthews, 2012]. Traumatic memories are associated with intense negative emotions; hence, emotion and memory are deeply interconnected in PTSD.

The striatum's role in generating a habit-like response to traumatic memories in PTSD has been well-documented [Cisler et al., 2014]. Increased, but less variable drive from the hippocampus to the striatum may underlie such a habit-like response. The precuneus is involved in generating the experience of visual memories, whereas the TPJ is involved in higher-level audio-visual information processing and verbalization [Gross, 2014]. Thus, the hippocampal memory-related network involving precuneus, TPJ and striatum likely translates the subcortical overdrive into elevated retrieval of traumatic memories, leading to trauma re-experiencing, hyperarousal, flashbacks and other such symptoms observed in soldiers with PTSD and PCS.

Taken collectively, we identified the MFG to be the pivotal source of network disruption in soldiers with PTSD and PCS (as all the connections could be traced back to this source), which further disinhibited emotion and memory processes, potentially exacerbating symptoms. The other two identified foci, insula and hippocampus, also play a critical role in mediating disruption, with the insula involved in subjective cognitive-emotional processing, and hippocampus involved in declarative memories. In

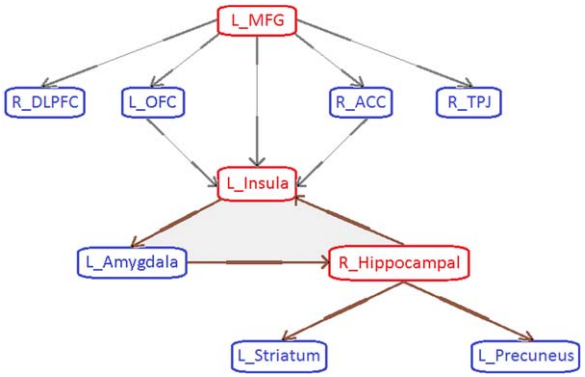

Figure 13.

Flowchart illustrating the aberrant effective connectivity network and the disrupted foci identified in this work. Paths with thin gray lines correspond to lower strength of connectivity (SEC) and lower variation in connectivity (vDEC) in the clinical groups compared to healthy controls, indicative of a breakdown in top-down modulation. Paths with thick brown lines correspond to higher SEC and lower vDEC, indicative of overdrive in subcortical limbic and parietal memory-related regions. Foci are in red, nonfoci are in blue. [Color figure can be viewed at wileyonlinelibrary.com]

concert, this network provides a mechanistic explanation of impaired cognitive control with emotion dysregulation and subsequent lack of control over traumatic memories, contributing to several symptoms observed in soldiers with PTSD and PCS. Figure 13 summarizes the findings with a flowchart.

Although progress in PTSD research seems to have arrived at some consensus on the pivotal role of MFG, our understanding of the relationship between PTSD and PCS is incomplete. Strong and reliable biomarkers that distinguish between the two disorders have yet to be developed [Simmons and Matthews, 2012]. However, we do know that mTBI appears to increase symptom severity in PTSD cases [Rangaprakash et al., 2017a,b,c; Vasterling et al., 2009]. In this study, we provide a mechanistic basis for behavioral observations, and explain network disturbances that describe and distinguish PTSD from comorbid PCS + PTSD.

Earlier studies have repeatedly identified these and other regions to be involved in both PTSD and PCS [Eierud et al., 2014; Hayes et al., 2012; Simmons and Matthews, 2012]. Yet, a precise understanding of the sources of network disruption, their subsequent causal relationships, and the underlying network structure has not emerged from them. Employing a novel framework involving foci identification and static/dynamic EC networks, we identified the regional foci associated with the disorders and elucidated their causal relationships. Our characterization fits well with behavioral manifestations of PTSD and PCS + PTSD, thus illustrating the utility and fidelity of our approach.

Additionally, connectivities of three of the paths exhibited significant associations with symptom severity and neurocognitive performance (MFG→insula, insula-amygdala, amygdala→hippocampus), thus highlighting the clinical relevance of these connectivity paths. The ensemble of connectivities could also explain about 57% variance in the ensemble of behaviors in the PLS regression model.

Our analysis framework to identify these disrupted foci and associated connections was based on statistical significance. Statistical significance, however, does not necessarily assure predictive ability of the identified connectivities [Pereira et al., 2009], because of which supervised machine learning classification was employed to classify between the three groups. Literature on machine learning applied to the classification of either PTSD or mTBI is highly limited (for notable recent works, see [Liu et al., 2015; Vergara et al., 2017]). In addition, there have been no studies that have employed machine learning to classify comorbid PTSD and mTBI. As one of our notable contributions, we performed machine learning classification, to find that the accuracies obtained using connectivity features were significantly higher (∼8% more) than nonimaging measures. Interestingly, we found that SEC and vDEC of these three paths (MFG→insula, insula→amygdala, amygdala→hippocampus), along with one other path not part of the network, resulted in the highest classification accuracy. In addition to being found statistically significant in accordance with our hypothesis, SEC and vDEC of these three paths were also identified as the top predictive features of diagnostic ability, over and above being behaviorally relevant through associations with symptom and neurocognitive scores. All these attributes were determined through a data-driven approach from whole-brain connectivity data, without the imposition of any priors or biases. With statistical significance, behavioral relevance and high predictive ability, these three connectivity paths could potentially be high-quality markers of neural and behavioral characteristics of PTSD and PCS. Importantly, these paths have potential as imaging biomarkers for these combat-related disorders, since they satisfy three of the four conditions described by Woo et al. [2015] necessary to be a good biomarker (diagnosticity, interpretability and deployability). Concerning the fourth condition (generalizability), based on suggestions in Woo *et al*., we issue an open call for researchers for sharing similar data for continued application of the classifier.

It is notable that ours is the first study to investigate either effective connectivity or dynamic connectivity in either PTSD or mTBI or the comorbid condition, and one among handful of studies to have utilized machine learning in either of these disorders. One of the novel contributions of this work lies in the use of dynamic connectivity as a marker or variability of connectivity, with lower variance of DEC in the clinical groups being the characteristic of all the connectivity paths identified in the network. In addition, given that our findings were obtained through an overlap/intersection of results for the PTSD and the PCS + PTSD groups, the observations and conclusions are

equally relevant to the study of PTSD alone. We posit that the novel framework used in this work is applicable to the study of any psychiatric illness or cognitive domain. We urge researchers to take advantage of this approach in identifying sources of disruption/alteration in various psychiatric illnesses and cognitive domains.

Finally, we present a number of caveats and limitations of this work, which demand careful interpretation of our findings, simultaneously suggesting directions for future studies: (1) The participants who sustained the added burden of PCS along with PTSD were found to have higher symptom severity than participants with PTSD alone, along with more extreme SEC and vDEC values. Though the literature on imaging studies of both PTSD and PCS are limited, we speculate that: (i) the added burden of a prior mTBI aggravates PTSD-related brain aberrations which were likely already prevalent before developing PCS in these participants, *or*, (ii) participants who sustained an mTBI and subsequently or concomitantly were exposed to a traumatic experience would end up with alleviated functional neural aberrations which correspond to elevated symptom severity, compared to participants who were exposed to psychological trauma alone. Future experimental designs could aim toward untangling the underlying cause-effect relationships in comorbid PTSD and PCS, in an effort to confirm either of the two scenarios. (2) Our study included military participants with combat exposure, which is a valuable contribution, given that it provides a more representative control group. A recent study found resting-state fMRI connectivity differences between healthy civilian and combat controls [Kennis et al., 2015], "potentially due to military training, deployment, and/or trauma exposure." Therefore, further work could verify whether our results are equally applicable to noncombat-related (or civilian) PCS and PTSD. (3) We did not collect specific details about frequency and temporal information of the mTBIs sustained during the specified period and lifetime. Hence, from the findings we can only infer that there are functional differences in soldiers being treated for postconcussive symptoms from one or more mTBI(s) compared to those with only PTSD and healthy controls. (4) One limitation is the reported differences in prescription medication between the groups, with the co-morbid group having the highest percentage of medicated participants. Due to the variety of medications being used by our subjects, and the range of associated pharmacodynamic and pharmacokinetic responses, it is not feasible to control for medication effects. Future studies should focus on medication-naïve participants to get a better understanding of the impact of PTSD and mTBI. (5) While performing RCE-SVM classification, we split our entire dataset into testing/validation (20%) and training (80%) datasets, giving us about seventeen participants (20% of 87) in the testing set; which is a comparatively small number for an fMRI connectivity study. (6) We studied only male veterans; hence, our findings cannot be generalized to female soldiers. (7) To make clinical use of the diagnostic utility of the connectivities in the future, the findings need to be replicated on a sample of much larger size, which is more representative of the target population in terms of gender, ethnicity, etc. (8) The data was acquired from the participants only on one instance. Longitudinal studies could develop hypotheses on the alterations of the connectivity network over the advancement, recovery and rehabilitation phases of the clinical groups. This would also be an appropriate test for validating the three pivotal connectivity paths (L_MFG → L_Insula, L_Insula → L_Amygdala, L_Amyg → R_Hippocampus) as candidate imaging biomarkers for PTSD and PCS + PTSD.

ACKNOWLEDGMENTS

The authors acknowledge financial support for this work from the U.S. Army Medical Research and Materials Command (MRMC) (Grant # 00007218). The views, opinions, and/or findings contained in this article are those of the authors and should not be interpreted as representing the official views or policies, either expressed or implied, of the U.S. Army or the Department of Defense (DoD). The funders had no role in study design, data collection and analysis, decision to publish, or preparation of the manuscript. The authors thank the personnel at the TBI clinic and behavioral health clinic, Fort Benning, GA, USA and the US Army Aeromedical Research Laboratory, Fort Rucker, AL, USA, and most of all, the soldiers who participated in the study. The authors thank Julie Rodiek and Wayne Duggan for facilitating data acquisition.

REFERENCES

Alba-Ferrara L, Hausmann M, Mitchell R, Weis S (2011): The neural correlates of emotional prosody comprehension: Disentangling simple from complex emotion. Plos One 6(12):e28701.

Amico E, Gomez F, Di Perri C, Vanhaudenhuyse A, Lesenfants D, Boveroux P, Bonhomme V, Brichant JF, Marinazzo d, Laureys S (2014): Posterior cingulate cortex-related co-activation patterns: A resting state FMRI study in propofol-induced loss of consciousness. PLoS One 9:e100012.

Bellucci G, Chernyak S, Hoffman M, Deshpande G, Monte OD, Knutson KM, Grafman J, Krueger F (2017): Effective connectivity of brain regions underlying third party punishment: Functional MRI and Granger causality evidence. Social Neurosci 12: 124–134.

Berlim M, Van Den Eynde F (2014): Repetitive transcranial magnetic stimulation over the dorsolateral prefrontal cortex for treating posttraumatic stress disorder: An exploratory meta-analysis of randomized, double-blind and sham-controlled trials. Can J Psychiatry 59:487–496.

Blevins C, Weathers F, Davis M, Witte T, Domino J (2015): The posttraumatic stress disorder checklist for DSM-5 (PCL-5): Development and initial psychometric evaluation. J Trauma Stress 28:489–498.

Boly M, Sasai S, Gosseries O, Oizumi M, Casali A, Massimini M, Tononi G (2015): Stimulus set meaningfulness and

neurophysiological differentiation: A functional magnetic resonance imaging study. PLoS One 10:e0125337.
Büchel C, Friston K (1998): Dynamic changes in effective connectivity characterized by variable parameter regression and Kalman filtering. Human Brain Mapping 6:403–408.
Cerullo M, Fleck D, Eliassen J, Smith M, DelBello M, Adler C, Strakowski S (2012): A longitudinal functional connectivity analysis of the amygdala in bipolar I disorder across mood states. Bipolar Disorders 14:175–184.
Chao-Gan Y, Yu-Feng Z (2010): DPARSF: A MATLAB toolbox for "pipeline" data analysis of resting-state fMRI. Front Syst Neurosci 4:13.
Chen G, Ward D, Xie C, Li W, Wu Z, Jones JL, Franczak M, Antuono P, Li S-J (2011): Classification of Alzheimer disease, mild cognitive impairment, and normal cognitive status with large-scale network analysis based on resting-state functional MR imaging. Radiology 259:213–221.
Cicerone K, Kalmar K (1995): Persistent postconcussion syndrome: The structure of subjective complaints after mild traumatic brain injury. J Head Trauma Rehabil 10:1–17.
Cisler J, Steele J, Lenow JK, Smitherman S, Everett B, Messias E, Kilts CD (2014): Functional reorganization of neural networks during repeated exposure to the traumatic memory in posttraumatic stress disorder: An exploratory fMRI study. J Psychiatr Res 48:47–55.
Costanzo ME, Chou YY, Leaman S, Pham DL, Keyser D, Nathan DE, Coughlin M, Rapp P, Roy MJ (2014): Connecting combat-related mild traumatic brain injury with posttraumatic stress disorder symptoms through brain imaging. Neuroscie Lett 577: 11–15.
Craddock R, Holtzheimer P, III, Hu X, Mayberg H (2009): Disease state prediction from resting state functional connectivity. Magn Reson Med 62:1619–1628.
Craddock R, James G, Holtzheimer P, Hu X, Mayberg H (2012): A whole brain fMRI atlas generated via spatially constrained spectral clustering. Hum Brain Mapp 33:1914–1928.
David O, Guillemain I, Saillet S, Reyt S, Deransart S, Segebarth C, Depaulis A (2008): Identifying neural drivers with functional MRI: An electrophysiological validation. PLoS Biol 23: 2683–2697.
Dempster A, Laird N, Rubin D (1977): Maximum likelihood from incomplete data via the EM algorithm. J R Stat Soc Series B (Methodol) 39:1–38.
Deshpande G, Hu X (2012): Investigating effective brain connectivity from fMRI data: Past findings and current issues with reference to Granger causality analysis. Brain Connectivity 2: 235–245.
Deshpande, G, James, G, Craddock, R, Mayberg HS, Hu X (2009). Predicting Treatment in Patients with Major Depression Using Granger-Based Connectivity and Support Vector Machines. *Proceedings of ISMRM 17th Scientific Meeting*, (p. p3362). Honolulu, HI.
Deshpande G, Li Z, Santhanam P, Coles CL, Hamann S, Hu X (2010): Recursive cluster elimination based support vector machine for disease state prediction using resting state functional and effective brain connectivity. PLoS One 5:e14277.
Deshpande G, Sathian K, Hu X (2010): Assessing and compensating for zero-lag correlation effects in time-lagged Granger causality analysis of FMRI. IEEE Trans Biomed Eng 57:1446–1456.
Deshpande G, Santhanam P, Hu X (2011): Instantaneous and causal connectivity in resting state brain networks derived from functional MRI data. Neuroimage 54:1043–1052.
Deshpande G, Sathian K, Hu X, Buckhalt J (2012): A rigorous approach for testing the constructionist hypotheses of brain function. Behav Brain Sci 35:148–149.
Deshpande G, Libero L, Sreenivasan K, Deshpande H, Kana R (2013): Identification of neural connectivity signatures of autism using machine learning. Front Hum Neurosci 17:670.
Deshpande G, Wang P, Rangaprakash D, Wilamowski B (2015): Fully connected cascade artificial neural network architecture for attention deficit hyperactivity disorder classification from functional magnetic resonance imaging data. IEEE Trans n Cybern 45:2668–2679.
Dickstein BD, Weathers FW, Angkaw AC, Nievergelt CM, Yurgil K, Nash WP, Baker DG, Litz BT, the Marine Resiliency Study Team (2014): Diagnostic utility of the posttraumatic stress disorder (PTSD) checklist for identifying full and partial PTSD in active-duty military. Assessment pii:1073191114548683.
Dretsch MN, Wood KH, Daniel TA, Katz JS, Deshpande G, Goodman AM, Wheelock MD, Wood KB, Denney TS, Traynham S, Knight D (2016): Exploring the neurocircuitry underpinning predictability of threat in soldiers with PTSD compared to deployment exposed controls. Open Neuroimage J 10:111–124.
Eierud C, Craddock R, Fletcher S, Aulakh M, King-Casas B, Kuehl D, LaConte S (2014): Neuroimaging after mild traumatic brain injury: Review and meta-analysis. NeuroImage Clin 4:283–294.
Emmert K, Kopel R, Sulzer J, Brühl AB, Berman BD, Linden DEJ, Horovitz SG, Breimhorst M, Caria A, Frank S, Johnston S, Long Z, Paret C, Robineau F, Veit R, Bartsch A, Beckmann CF, Van De Ville D, Haller S (2016): Meta-analysis of real-time fMRI neurofeedback studies using individual participant data: How is brain regulation mediated?. Neuroimage 124:806–812.
Feng C, Deshpande G, Liu C, Gu R, Luo Y-J, Krueger F (2015): Diffusion of responsibility attenuates altruistic punishment: A functional magnetic resonance imaging effective connectivity study. Hum Brain Mapp 37:663–677.
Friston K, Ashburner J, Kiebel S, Nichols T, Penny W (2007): Statistical Parametric Mapping: The Analysis of Functional Brain Images. Academic Press. Retrieved from http://www.fil.ion.ucl.ac.uk/spm
Friston K, Harrison L, Penny W (2013): Dynamic causal modelling. Neuroimage 19:1273–1302.
Garrett D, Samanez-Larkin G, MacDonald S, Lindenberger U, McIntosh A, Grady C (2013): Moment-to-moment brain signal variability: A next frontier in human brain mapping? Neurosci Biobehav Rev 37:610–624.
Granger C (1969): Investigating causal relations by econometric models and cross-spectral methods. Econometrica 37:424–438.
Grant M, White D, Hadley J, Hutcheson N, Shelton R, Sreenivasan K, Deshpande G (2014): Early life trauma and directional brain connectivity within major depression. Hum Brain Mapp 35:4815–4826.
Grant MM, Wood K, Sreenivasan KR, Wheelock M, White D, Thomas J, Knight DC, Deshpande G (2015): Influence of early life stress on intra- and extra-amygdaloid causal connectivity. Neuropsychopharmacology 40:1782–1793.
Gray M, Litz B, Hsu J, Lombardo T (2004): Psychometric properties of the life events checklist. Assessment 11:330–341.
Greiser KH, Kluttig A, Schumann B, Swenne CA, Kors JA, Kuss O, Haerting J, Schmidt H, Thiery J, Werdan K (2009): Cardiovascular diseases, risk factors and short-term heart rate variability in an elderly general population: The CARLA study 2002–2006. Eur J Epidemiol 24:123–142.

Gross J (2014): Handbook of Emotion Regulation. New York: The Guilford Press.

Gualtieri C, Johnson L (2006): Reliability and validity of a computerized neurocognitive test battery, CNS Vital Signs. Arch Clin Neuropsychol 21:623–643.

Guyker WM, Donnelly K, Donnelly JP, Dunnam M, Warner GC, Kittleson J, Bradshaw CB, Alt M, Meier ST (2013): Dimensionality, reliability, and validity of the combat experiences scale. Mil Med 178:377–384.

Hall C, Howarth C, Kurth-Nelson Z, Mishra A (2016): Interpreting BOLD: Towards a dialogue between cognitive and cellular neuroscience. Philos Trans R Soc Lond B 371:20150348.

Handwerker D, Ollinger J, D'Esposito M (2004): Variation of BOLD hemodynamic responses across subjects and brain regions and their effects on statistical analyses. Neuroimage 21:1639–1651.

Hansen E, Battaglia D, Spiegler A, Deco G, Jirsa V (2015): Functional connectivity dynamics: Modeling the switching behavior of the resting state. Neuroimage 105:525–535.

Hayes J, Vanelzakker M, Shin L (2012): Emotion and cognition interactions in PTSD: A review of neurocognitive and neuroimaging studies. Front Integr Neurosci 6:89.

Hillary F, Roman C, Venkatesan U, Rajtmajer SM, Bajo R, Castellanos ND (2015): Hyperconnectivity is a fundamental response to neurological disruption. Neuropsychology 29:59–75.

Hoge CW, Castro C, Messer SC, McGurk D, Cotting DI, Koffman RL (2008): Mild traumatic brain injury in U.S. soldiers returning from Iraq. N Engl J Med 358:453–463.

Hoge CW, Goldberg HM, Castro CA (2009): Care of war veterans with mild traumatic brain injury: Flawed perspectives. N Engl J Med 360:1588–1591.

Hutchison RM, Womelsdorf T, Allen EA, Bandettini PA, Calhoun VD, Corbetta M, Della PS, Duyn JH, Glover GH, Gonzalez-Castillo J, Handwerker DA, Keilholz S, Kiviniemi V, Leopold DA, de Pasquale F, Sporns O, Walter M, Chang C (2013): Dynamic functional connectivity: Promise, issues, and interpretations. Neuroimage 80:360–378.

Hutcheson NL, Sreenivasan KR, Deshpande G, Reid MA, Hadley J, White DM, Ver Hoef L, Lahti AC (2015): Effective connectivity during episodic memory retrieval in schizophrenia participants before and after antipsychotic medication. Hum Brain Mapp 36: 1442–1457.

Illari P, Russo F, Williamson J. (2011): Causality in the Sciences. New York: Oxford University Press.

Jia H, Hu X, Deshpande G (2014): Behavioral relevance of the dynamics of the functional brain connectome. Brain Connectivity 4:741–759.

Jin C, Jia H, Lanka P, Rangaprakash D, Li L, Liu T, Hu X, Deshpande G (2017): Dynamic brain connectivity is a better predictor of PTSD than static connectivity. Hum Brain Mapp 38:4479–4496.

Johns M (1991): A new method for measuring daytime sleepiness: The Epworth sleepiness scale. Sleep 14:540–545.

Kaminski M, Ding M, Truccolo W, Bressler S (2001): Evaluating causal relations in neural systems: Granger causality, directed transfer function and statistical assessment of significance. Biol Cybern 85:145–157.

Katwal S, Gore J, Gatenby J, Rogers B (2013): Measuring relative timings of brain activities using fMRI. Neuroimage 66:436–448.

Kennis M, Rademaker A, van Rooij S, Kahn R, Geuze E (2015): Resting state functional connectivity of the anterior cingulate cortex in veterans with and without post-traumatic stress disorder. Hum Brain Mapp 36:99–109.

King D, King L, Vogt D (2003): Manual for the Deployment Risk and Resilience Inventory (DRRI): A Collection of Measures for Studying Deployment-Related. Boston, MA: National Center for PTSD.

Kirchgässner G, Wolters J, Hassler U (2012): Introduction to Modern Time Series Analysis. New York: Springer.

Kriegeskorte N, Simmons W, Bellgowan P, Baker C (2009): Circular analysis in systems neuroscience: The dangers of double dipping. Nat Neurosci 12:535–540.

Krishnan A, Williams L, McIntosh A, Abdi H (2011): Partial Least Squares (PLS) methods for neuroimaging: A tutorial and review. Neuroimage 56:455–475.

Lacey S, Stilla R, Sreenivasan K, Deshpande G, Sathian K (2014): Spatial imagery in haptic shape perception. Neuropsychologia 60:144–158.

Lamichhane B, Adhikari B, Brosnan S, Dhamala M (2014): The neural basis of perceived unfairness in economic exchanges. Brain Connectivity 4:619–630.

Liu F, Xie B, Wang Y, Guo W, Fouche JP, Long Z, Wang W, Chen H, Li M, Duan X, Zhang J, Qiu M, Chen H (2015): Characterization of post-traumatic stress disorder using resting-state fMRI with a multi-level parametric classification approach. Brain Topogr 28:221–237.

Lohmann G, Erfurth K, Müller K, Turner R (2012): Critical comments on dynamic causal modelling. Neuroimage 59:2322–2329.

Marquand A, Filippone M, Ashburner J, &, et.al. (2013): Automated, high accuracy classification of Parkinsonian disorders: A pattern recognition approach. PLoS One 8:e69237.

Miller R, Yaesoubi M, Turner J, Mathalon D, Preda A, Pearlson G, al e (2016): Higher dimensional meta-state analysis reveals reduced resting fMRI connectivity dynamism in Schizophrenia patients. PLoS One 11:e0149849.

Modinos G, McLaughlin A, Egerton A, McMullen A, Kumari V, Barker GJ, Keysers C, Williams SC (2017): Corticolimbic hyperresponse to emotion and glutamatergic function in people with high schizotypy: A multimodal fMRI-MRS study. Transl Psychiatry 7:e1083.

Oishi K, Faria A, Hsu J, Tippett D, Mori S, Hillis A (2015): Critical role of the right uncinate fasciculus in emotional empathy. Ann Neurol 77:68–74.

Pereira F, Mitchell T, Botvinick M (2009): Machine learning classifiers and fMRI: A tutorial overview. Neuroimage 45:S199–S209.

Power J, Barnes K, Snyder A, Schlaggar B, Petersen S (2012): Spurious but systematic correlations in functional connectivity MRI networks arise from subject motion. Neuroimage 59:2142–2154.

Rangaprakash D, Deshpande G, Daniel TA, Goodman A, Katz JS, Salibi N, Denney TS, Dretsch MN (2015): Static and dynamic functional connectivity impairments in concussed soldiers with and without PTSD. Proc Annu Meeting Int Soc Magn Reson Med 23:4402.

Rangaprakash D, Deshpande G, Venkataraman A, Katz J, Denney T, Dretsch M (2016): Identifying foci of brain disorders from effective connectivity networks. Proc Annu Meeting Int Soc Magn Reson Med 24:3740.

Rangaprakash D, Dretsch MN, Yan W, Katz JS, Denney TS, Deshpande G (2017a): Hemodynamic response function parameters obtained from resting-state functional MRI data in soldiers with trauma. Data in Brief 14:558–562.

Rangaprakash D, Dretsch MN, Yan W, Katz JS, Denney TS, Deshpande G (2017b): Hemodynamic variability in soldiers with trauma: Implications for functional MRI connectivity studies. NeuroImage: Clinical 16:409–417.

Rangaprakash D, Deshpande G, Daniel TA, Goodman AM, Robinson JL, Salibi N, Katz JS, Denney JS, Dretsch MN (2017c): Compromised hippocampus-striatum pathway as a potential imaging biomarker of mild traumatic brain injury and post-traumatic stress disorder. Hum Brain Map 38:2843–2864.

Rashid B, Arbabshirani M, Damaraju E, Cetin M, Miller R, Pearlson G, Calhoun V (2016): Classification of schizophrenia and bipolar patients using static and dynamic resting-state fMRI brain connectivity. NeuroImage 134:645–657.

Reiss A, Hoeft F, Tenforde A, Chen W, Mobbs D, Mignot E (2008): Anomalous hypothalamic responses to humor in cataplexy. PLoS One 3:e2225.

Roebroeck A, Formisano E, Goebel R (2005): Mapping directed influence over the brain using Granger causality and fMRI. Neuroimage 25:230–242.

Rolls E, Grabenhorst F, Parris B (2008): Warm pleasant feelings in the brain. Neuroimage 41:1504–1513.

Ryali S, Supekar K, Chen T, Menon V (2011): Multivariate dynamical systems models for estimating causal interactions in fMRI. Neuroimage 54:807–823.

Ryali S, Chen T, Supekar K, Menon V (2012): Estimation of functional connectivity in fMRI data using stability selection-based sparse partial correlation with elastic net penalty. Neuroimage 59:3852–3861.

Ryali S, Shih YY, Chen T, Kochalka J, Albaugh D, Fang Z, Supekar K, Lee JH, Menon V (2016): Combining optogenetic stimulation and fMRI to validate a multivariate dynamical systems model for estimating causal brain interactions. Neuroimage 132:398–405.

Sakoğlu U, Pearlson G, Kiehl K, Wang Y, Michael A, Calhoun V (2010): A method for evaluating dynamic functional network connectivity and task-modulation: Application to schizophrenia. MAGMA 23:351–366.

Sathian K, Deshpande G, Stilla R (2013): Neural changes with tactile learning reflect decision level reweighting of perceptual readout. J Neurosci 33:5387–5398.

Saunders J, Aasland O, Babor T, de la Fuente J, Grant M (1993): Development of the alcohol use disorders identification test (AUDIT): WHO Collaborative Project on early detection of persons with harmful alcohol consumption–II. Addiction 88:791–804.

Schwab KA, Ivins B, Cramer G, Johnson W, Sluss-Tiller M, Kiley K, Lux W, Warden D (2007): Screening for traumatic brain injury in troops returning from deployment in Afghanistan and Iraq: Initial investigation of the usefulness of a short screening tool for traumatic brain injury. J Head Trauma Rehabil 22:377–389.

Simmons A, Matthews S (2012): Neural circuitry of PTSD with or without mild traumatic brain injury: A meta-analysis. Neuropharmacology 62:598–606.

Song XM, Dong ZY, Long XY, Li SF, Zuo XN, Zhu CZ, He Y, Yan CG, Zang YF (2011): REST: A toolkit for resting-state functional magnetic resonance imaging data processing. PLoS One 6:e25031.

Spielberg J, McGlinchey R, Milberg W, Salat D (2015): Brain network disturbance related to posttraumatic stress and traumatic brain injury in veterans. Biol Psychiatry 78:210–216.

Squire L, Wixted J (2011): The cognitive neuroscience of human memory since H.M. Annu Rev Neurosci 34:259–288.

Thayer J, Lane R (2000): A model of neurovisceral integration in emotion regulation and dysregulation. J Affect Disord 61: 201–216.

Vapnik V (1995): The Nature of Statistical Learning Theory. New York: Springer.

Vasterling J, Verfaellie M, Sullivan K (2009): Mild traumatic brain injury and posttraumatic stress disorder in returning veterans: Perspectives from cognitive neuroscience. Clin Psychol Rev 29:674–684.

Venkataraman A, Kubicki M, Golland P (2013): From connectivity models to region labels: Identifying foci of a neurological disorder. IEEE Trans Med Imaging 32:2078–2098.

Vergara V, Mayer A, Damaraju E, Kiehl K, Calhoun V (2017): Detection of mild traumatic brain injury by machine learning classification using resting state functional network connectivity and fractional anisotropy. J Neurotrauma 34:1045–1053.

Veterans statistics: PTSD, Depression, TBI, Suicide. (n.d.). Retrieved November 2015, from http://www.veteransandptsd.com/PTSD-statistics.html

Wang L (2005): Support Vector Machines: Theory and Applications. New York: Springer.

Weathers, F., Litz, B., Keane, T., Palmieri, P., Marx, B., & Schnurr, P. (2015). *The PTSD Checklist for DSM-5 (PCL-5)*. Retrieved 05 01, 2015, from Scale available from the National Center for PTSD at www.ptsd.va.gov

Wen X, Rangarajan G, Ding M (2013): Is Granger causality a viable technique for analyzing fMRI data? PLoS One 8:e67428.

Wheelock M, Sreenivasan K, Wood K, Ver Hoef L, Deshpande G, Knight D (2014): Threat-related learning relies on distinct dorsal prefrontal cortex network connectivity. Neuroimage 102:904–912.

White S, Costanzo M, Blair J, Roy M (2014): PTSD symptom severity is associated with increased recruitment of top-down attentional control in a trauma-exposed sample. Neuroimage Clin 7:19–27.

Woo C, Wager T (2015): Neuroimaging-based biomarker discovery and validation. Pain 156:1379–1381.

Wu G, Liao W, Stramaglia S, Ding J, Chen H, Marinazzo D (2013): A blind deconvolution approach to recover effective connectivity brain networks from resting state fMRI data. Med Image Anal 17:365–374.

Xia M, Wang J, He Y (2013): BrainNet Viewer: A network visualization tool for human brain connectomics. PLoS One 8:e68910.

Yousef M, Jung S, Showe L, Showe M (2007): Recursive Cluster Elimination (RCE) for classification and feature selection from gene expression data. BMC Bioinformatics 8:144.

Zhang J, Cheng W, Liu Z, Zhang K, Lei X, Yao Y, Becker B, Liu Y, Kendrick KM, Lu G, Feng J (2016): Neural, electrophysiological and anatomical basis of brain-network variability and its characteristic changes in mental disorders. Brain 139: 2307–2321.

Zhao S, Rangaprakash D, Venkataraman A, Liang P, Deshpande G (2017): Investigating focal connectivity deficits in Alzheimer's disease using directional brain networks derived from resting-state fMRI. Front Aging Neurosci 9:211.

Zung W (1971): A rating instrument for anxiety disorders. Psychosomatics 12:371–379.

Zung W, Richards C, Short M (1965): Self-rating depression scale in an outpatient clinic. Further validation of the SDS. Arch Gen Psychiatry 13:508–515.